Heliyon 10 (2024) e39206

Contents lists available at ScienceDirect

Heliyon

journal homepage: www.cell.com/heliyon

Research article

Plasma C24:0 ceramide impairs adipose tissue remodeling and promotes liver steatosis and glucose imbalance in offspring of rats

Alberto Camacho-Morales [a,b,*], Lilia G. Noriega [c], Adriana Sánchez-García [d], Ivan Torre-Villalvazo [c], Natalia Vázquez-Manjarrez [c], Roger Maldonado-Ruiz [a,b], Marcela Cárdenas-Tueme [e], Mariana Villegas-Romero [c], Itzayana Alamilla-Martínez [c], Humberto Rodriguez-Rocha [f], Aracely Garcia-Garcia [f], Juan Carlos Corona [g], Armando R. Tovar [c], Jennifer Saville [h], Maria Fuller [h], José Gerardo Gonzalez-Gonzalez [d], Ana María Rivas-Estilla [a]

[a] *Biochemistry and Molecular Medicine Department, College of Medicine, Autonomous University of Nuevo Leon, Monterrey, Mexico*
[b] *Neurometabolism Unit, Center for Research and Development in Health Sciences, Autonomous University of Nuevo Leon, Monterrey, Mexico*
[c] *Nutrition Physiology Department, National Institute of Medical Sciences and Nutrition. México City, Mexico*
[d] *University Hospital "Dr. Jose E. Gonzalez, Endocrinology Division. Department of Internal Medicine. Autonomous University of Nuevo Leon Monterrey, Mexico*
[e] *Facultad de Salud Pública y Nutrición, Centro de Investigación en Nutrición y Salud Pública, Universidad Autónoma de Nuevo León, Monterrey, Mexico*
[f] *Histology Department, College of Medicine, Autonomous University of Nuevo Leon, Monterrey, Mexico*
[g] *Neuroscience Laboratory, Hospital Infantil de México, Federico Gómez, México City, Mexico*
[h] *Genetics and Molecular Pathology, SA Pathology at Women's and Children's Hospital, University of Adelaide, Australia*

ARTICLE INFO

Keywords:
Diabetes
C24:0 ceramide
fetal programming
Adipose tissue remodeling
mitochondria
ER stress

ABSTRACT

Fetal programming by exposure to high-energy diets increases the susceptibility to type 2 diabetes mellitus (T2DM2) in the offspring. Glucose imbalance during fetal programming might be associated to still unknown selective lipid species and their characterization might be beneficial for T2DM diagnosis and treatment. We aim to characterize the effect of the lipid specie, C24:0 ceramide, on glucose imbalance and metabolic impairment in cellular and murine models. A lipidomic analysis identified accumulation of C24:0 ceramide in plasma of offspring rats exposed to high-energy diets during fetal programing, as well as in obese-T2DM subjects. *In vitro* experiments in 3T3L-1, hMSC and HUH7 cells and in *in vivo* models of Wistar rats and C57BL/6 mice demonstrated that C24:0 ceramide disrupted glucose balance, and differentiation and lipid accumulation in adipocytes, whereas promoted liver steatosis. Mechanistically, C24:0 ceramide impaired mitochondrial fatty acid oxidation in adipocytes and hepatic cells, tentatively by favoring reactive oxygen species accumulation and calcium overload in the mitochondria; and also, activates endoplasmic reticulum (ER) stress in hepatocytes. We propose that C24:0 ceramide accumulation in the offspring followed a prenatal diet exposure, impair lipid allocation into adipocytes and enhances liver steatosis associated to mitochondrial dysfunction and ER stress, leading to glucose imbalance.

* Corresponding author. Biochemistry and Molecular Medicine Department, College of Medicine. Autonomous University of Nuevo Leon. Ave. Francisco I Madero y Dr. Eduardo Aguirre Pequeño s/n. Colonia Mitras Centro. Monterrey, Mexico. C.P. 64460.
E-mail addresses: acm590@hotmail.com, alberto.camachomr@uanl.edu.mx (A. Camacho-Morales).

https://doi.org/10.1016/j.heliyon.2024.e39206
Received 24 December 2023; Received in revised form 8 October 2024; Accepted 9 October 2024
Available online 11 October 2024

1. Introduction

The Developmental Origins of Health and Disease (DOHaD) theory states that external stimuli during early life (prenatal stage) can permanently program the health or disease in later life [1]. Accordingly, maternal obesity and/or maternal overnutrition in humans associates with an increased risk of metabolic-related disorders in the offspring [2]. In previous reports, we identified that maternal programming by exposure to energy-dense diets promotes overfeeding [3,4], obesity and type 2 diabetes mellitus (T2DM) [5] and addiction-like behavior phenotypes for food intake in the offspring [6,7]. Of note, maternal programming by high-energy diets sets a plasma lipidomic signature in the offspring which correlates with glucose intolerance, insulin resistance and liver steatosis [4,7–9].

Lipidomic characterization of plasma from obese individuals identified accumulation of lysophosphatidylcholines, C18:0 ceramide and dihydroceramides, which associate with T2DM [11–14]. Ceramide are synthetized by De novo pathway which begins with the condensation of l-serine and a fatty-acyl CoA such as palmitoyl- CoA, myristoyl CoA, or stearoyl CoA at the endoplasmic reticulum in the brain, liver, kidney, skin, heart, leukocytes, and intestine [15,16]. Accordingly, exposure to high-fat diets in humans increases circulating d18:0–24:0, d18:1–24:0 and 24:1 ceramides species [13]. Accumulation of C16:0 and C18:0 in murine models of obesity leads to increased body weight gain, insulin resistance and glucose intolerance [17–19], whereas a reduction in C16:0 and C18:0 ceramides trough deletion of ceramide synthesizing enzymes improves insulin sensitivity and glucose metabolism [17–19]. Mechanistically, C16:0 ceramide seems to bind to the mitochondrial fusion protein MFN2 promoting mitochondria fragmentation and insulin resistance [17]. In fact, C16:0 disrupts mitochondrial dynamics in different disease models including preeclampsia [20], carcinoma [21], and cardiac dysfunction [22]. Notably, we and others reported that defective mitochondria dynamics prompts the development of metabolic disorders in obese mice [23–25], and in the offspring of mothers exposed to energy-dense diets during gestation [26,27]. Also, ceramides disrupt the insulin signaling pathway (IRS, Akt) in several metabolic-associated tissues affecting glucose balance [28]. These data suggest that prenatal exposure to energy-dense diets primes ceramides accumulation in the plasma of offspring, negatively modulating mitochondria dynamics and favoring metabolic disturbances. However, a cause-effect relationship between prenatal programming, early synthesis of selective ceramides species and glucose imbalance has not been fully established.

Ectopic lipid accumulation in tissues such as the liver, skeletal muscle and the heart leads to lipotoxic cell death. To prevent lipotoxicity, excess lipids are safely stored in white adipose tissue (WAT), which can undergo substantial cellular and structural remodeling aiming at optimizing its storage capacity to allocate nutrients overload as a response to increased energy intake [29]. However, once WAT expansion limit is reached, adipocyte differentiation decreases, and adipocytes become hypertrophic preventing further fat storage. Increased lipolysis in hypertrophic adipose tissue leads to fat accumulation in ectopic organs, causing metabolic derangements [29]. Seminal reports in cellular and murine models documented that ectopic accumulation of ceramides is a major trigger of lipotoxic damage favoring insulin resistance and glucose imbalance [30–32]. However, the current literature has not identified the ceramide species involved in the disruption of adipose tissue remodeling or glucose imbalance during prenatal stages. Also, these studies fail in describing a mechanism for impaired mitochondrial dynamics during adipose tissue dysfunction.

In the current study, we identified the C24:0 ceramide in plasma of both offspring of rats exposed to high-energy diets during gestation and in obese-T2DM subjects, as a lipid specie that induces adipose tissue dysfunction. Herein, we provided direct evidence using *in vitro* and *in vivo* models that plasma C24:0 ceramide disrupts lipid accumulation in adipose tissue and induces hepatic steatosis trough impairment of mitochondrial function in adipocytes and hepatocytes as well as inducing ER stress in hepatocytes.

2. Materials and Methods

2.1. Obese and T2DM human cohorts

All participants provided written informed consent under protocols approved by the institutional review board at the Universidad Autónoma de Nuevo Leon, México and were conducted in accordance with the Declaration of Helsinki of the World Medical Association. Participants were included into two cohorts: Cohort 1, insulin-sensitive obese subjects (Women n = 40, Male n = 20); Cohort 2, insulin-resistant obese-type 2 diabetes mellitus (T2DM) subjects (Women n = 34, Male n = 18). Inclusion criteria for obese cohort was 18–70 years aged and BMI ≥30 kg/m2. Inclusion criteria for the obese-T2DM cohort according to the American Diabetes Association was 18–70 years aged, BMI ≥30, fasting glucose ≥126 mg/dL (7.0 mmol/L), post prandial plasma glucose ≥200 mg/dL (11.1 mmol/L) after a 75-g oral glucose load, HbA1c levels ≥6.5 % (48 mmol/mol), T2DM evolution no longer than 6 months. None of the patients received insulin treatment, metformin and/or sulfonylureas.

2.2. Animals and experimental design

2.2.1. Diets

The control diet was standard chow containing 57 % carbohydrates, 13 % lipids, and 30 % proteins, caloric density = 3.35 kcal/g (LabDiet, St. Louis). The cafeteria (CAF) diet was made of liquid chocolate, biscuits, bacon, fries potatoes, standard diet, and pork paté based on a 1:1:1:1:1:2 ratio, respectively; total calories 3.72 kcal/g in 39 % carbohydrates, 49 % lipids, 12 % proteins, and 513.53 mg of sodium, caloric density = 3.72 kcal/g, as we reported before [3,5,6,33–37].

2.2.2. Fetal programming model in Wistar rats

We used two-month-old wild-type female (200–250 g) or male (250–300 g) Wistar rats, or two-month-old wild-type male C57BL/6

mice (25–30 g). Animals were maintained and used in accordance with the guidelines of the Institutional Animal Care facility and was approved by the local Animal Care Committee (BI0002). Rats or mice were housed individually in Plexiglas-style cages, maintained at 20–23 °C in a temperature-controlled room with a 12-h light/dark cycle. Water was available *ad libitum* in the home cage.

For the fetal programming protocol, we followed the reported experimental procedures [3,5,6,33–37]. In brief, virgin female rats (n = 10) were randomly divided in two batches; one was fed *ad libitum* with control diet (Control group, n = 4), and the second was fed the CAF diet (CAF group, n = 6) for 9 weeks (pre-pregnancy, pregnancy and lactation). Rats were mated with age matched Wistar males for two days, after which males were removed from the home cage. Pregnancy diagnosis was performed in females after mating by vaginal plug. Female rats lacking copulation plugs were returned to the home cage for a second mating. Pregnant rats were kept on the same diet after birth and during lactation. Male offspring were weaned at post-natal day 21, divided in three groups of 10–12 animals. Offspring of rats fed the control diet were maintained in the control diet (Control), whereas offspring of rats fed the CAF diet were divided in two groups; one was fed the control diet (CAF-Control) ant the other was fed the CAF diet (CAF-CAF). Body weight and food intake were measured weekly during the experiment (see Fig. 2A). Female offspring were allocated to a second experimental protocol currently active.

2.2.3. Chronic C24:0 ceramide administration in mice

Ceramide 24:0 stock solution was dissolved in dimethyl sulfoxide (DMSO) and diluted 1:2 final ratio in free fatty acid-bovine serum albumin. Ceramide 24:0 stock was mix with saline 1:2 final ratio in fatty acid free-bovine serum albumin (FAF-BSA) as described below. Control mice were administered with saline 1:2 in FAF-BSA. The effect of chronic ceramide 24:0 administration on glucose metabolism, adipose tissue remodeling, insulin secretion and mitochondria dynamics was evaluated in two experiments as follow:

Experiment 1: effect of chronic C24:0 administration on glucose and weight homeostasis: Two-month-old wild-type C57BL/6 male mice were allocated into two groups: Control (saline, n = 10) and C24:0 ceramide (n = 12). Daily intraperitoneal injections of saline (100 μL) or C24:0 ceramide (3.5 nmol/ml), respectively, were performed for 4 weeks. Food intake and body weight were recorded daily, and intraperitoneal glucose tolerance and insulin tolerance test (ipGTT, ipITT) assessments were evaluated at 3rd and 4th weeks, respectively, as described below. Food efficiency ratio was evaluated by analyzing total food intake divided into body weight change (total food intake/final weight - starting weight). Mice were euthanized at 5th week (see Fig. 3A). Ceramide dose was based on previous reports documented in plasma of C57BL/6 mice [38].

Experiment 2: effect of chronic C24:0 administration on glucose and weight homeostasis and adipose tissue remodeling. Two-month-old wild-type C57BL/6 male mice were allocated into two groups as follow: Control (saline, n = 20) and C24:0 ceramide (n = 24), as described in Experiment 1. Followed Saline or C24:0 administration, animals were fed either the control or the CAF diet for 4 weeks. Food intake and body weight were recorded daily, and GTT and ITT assessments were evaluated at 7th and 8th weeks, respectively, as described below. Mice were euthanized at 9th week (see Fig. 4A).

2.2.4. Intraperitoneal glucose tolerance and insulin tolerance test (ipGTT, ipITT) assessments

Mice were food-deprived for 8 h–12 h and were i.p. injected with 40 % glucose or 1 U of insulin/100 g body weight for ipGTT and ipITT evaluation, respectively. Blood glucose levels were quantified from a drop of blood from the caudal vein, using a glucometer (Accu-Check, Cat. 05987270, Roche) at 0 min, 15 min, 30 min, 60 min, 90 min, and 120 min, as described previously [3,5]. Blood samples were also obtained at 0 min, 15 min, 30 min and 60 min, during the GTT. Serum was obtained by centrifugation at 1300 rfc x 10 min at 4 °C and insulin levels were determined by ELISA (Rat/Mouse Insulin ELISA, Merck Millipore).

2.3. Rat and mice blood and tissue collection and human plasma collection

Male rats and mice were food-deprived overnight and euthanized by decapitation at 9th weeks of age, respectively. Blood samples were collected in 500 μL tubes (Beckton Dickinson), plasma fraction was separated by centrifugation at 1300 rfc x 10 min at 4 °C and stored at − 80 °C. Liver, white adipose tissue and skeletal muscle were dissected, snap-frozen in liquid nitrogen and stored at − 80 °C.

Venous blood samples from obese and T2DM subjects were collected by an experienced phlebotomists after an 8–12 h overnight fasting in 5 ml tubes (BD Vacutainer- Ethylenediaminetetraacetic acid). Plasma fraction was separated by centrifugation as described and stored at − 80 °C.

2.4. Mass spectrometric determinations of ceramides and acyl glycerides

Lipids were extracted from 10 μL of human or mouse plasma as previously described in Fuller et al. [39], with the exception that 20 pmol of 1,3-dipentadecanoylglycerol (DG (15:0/15:0); Sigma-Aldrich, St. Louis, MO, USA) and 10 pmol of N-heptadecanoyl-D-erythro-sphingosine (Cer (d18:1/17:0); Avanti Polar Lipids Inc., Alabaster, AL, USA) were added as internal standards. Extracted ceramide (Cer) and diacylglycerol (DG) were quantified by liquid chromatography electrospray ionization tandem mass spectrometry (LC-ESI-MS/MS) as previously described [40]. Individual species were measured by multiple reaction monitoring (MRM) with Cer transitions, while DG species were measured using the ammonium adduct and fragment arising from the neutral loss of one fatty acid. DG species were named with an underscore where the sn position of the fatty acid could not be determined. Thirty eight DG transitions were monitored with 12 observed in mouse plasma: 16:0_18:2 (610.5/313.3), 16:0_20:4 (634.5/313.3), 16:0_22:6 (658.5/313.3), 18:0_18:1 (640.6/339.3), 18:0_18:2 (638.6/341.3), 18:0_20:4 (662.6/341.3), 18:1/18:1 (638.6/339.3), 18:1_16:0 (612.6/339.3), 18:1_18:2 (636.6/339.3), 18:1_18:3 (634.5/339.3), 18:1_20:4 (660.6/339.3), 18:2/18:2 (634.5/337.3). Concentrations were determined by relating the peak area of each species to that of the internal standard using MultiQuant software (v. 3.0.1; AB SCIEX,

Framingham, MA, USA).

2.5. Oil red staining for lipid accumulation and Hematoxylin and Eosin staining (H&E) in tissue sections

Liver and subcutaneous adipose tissue (SAT) samples were fixed in 10 % formaldehyde and morphological analysis were performed as reported [41].

2.6. Morphometric analysis of adipose tissue

Adipocyte diameter was assessed on randomly chosen H&E-stained slides in nine planes for saline or C24:0 ceramide groups. We analyzed sixty adipocytes per group. Microphotography's show 20X and 40× magnification after.

2.7. Isolation of adipocytes from WAT and measurements of mitochondrial membrane potential ($\Delta\Psi m$) and reactive oxygen species (ROS) generation

Mouse subcutaneous adipocytes were isolated as described [42] with minor modifications. In brief, after euthanasia inguinal SAT fat pads were dissected and minced carefully with scissors until no obvious tissue pieces were visible. The minced tissue was digested in a 37 °C shaking water bath at 200 rpm with 10 mL Phosphate Buffer Saline (PBS) containing 1 % bovine serum albumin (BSA), 2 mg/ml Dispase II (Sigma) and 2 mg/ml Collagenase D (Roche). Afterwards, the digested tissue was filtered through a 100 mm nylon mesh strainer and washed 3 times using a total of 40 mL wash buffer (1 % BSA in PBS, pH 7.4) at room temperature. After every round of washing, adipocytes were allowed to float for 3–5 min and the infranatant was carefully removed using a Pasteur pipette. Finally, a sample of isolated adipocytes was filtered using a 100 mm nylon mesh strainer in PBS for H&E staining.

Mitochondrial membrane potential in primary adipocytes was measured using tetramethylrhodamine, Ethyl Ester, Perchlorate (TMRE; Sigma, Aldrich, Darmstadt, Germany) and ROS production levels were measured using dihydroethidium (DHE; Invitrogen, St Louis, MO, USA) for $O2-$ quantification by flow cytometry. In brief, isolated adipocytes were stained with BODIPY (2 μM, Thermofisher) TMRE (100 nM, Thermofisher) or DHE (1 μM) and incubated for 30 min at 37 °C. Later, adipocytes were rinsed once in PBS and analyzed by flow cytometry (BD Accuri C6) using the FL1 for BODIPY+ and the FL3 channel for TMRE + or DHE+. All of the events that were positive for the FL1 channel were considered as adipocytes and that is where we measured the loss of mitochondrial potential or ROS production using the BD Accuri C6 software.

2.8. Cell culture

The 3T3-L1 mouse preadipocyte cell line (ATCC, Manassas, Virginia), human mesenchymal stem cells (hMSC) and HUH7 cells were expanded in Dulbecco's modified Eagle's medium (DMEM high glucose 4.5 g/l, Caisson Labs, EEUU, Utah), 10 % (vol/vol) newborn calf serum (Fetal Bovine Serum, Sigma Aldrich, EE.UU, Missouri), 50 units/ml penicillin, and 50 μg/ml streptomycin (Penicillin/Streptomycin, Sigma Aldrich, EE.UU, Missouri) in 5 % CO2 incubator at 37 °C. After confluence, 3T3-L1 and hMSC cells were induced to adipocyte differentiation for 14 days by using DMEM supplemented 1 μM dexamethasone, 0.5 mM isobutylmethylxanthine and 100 nM insulin as we reported previously [41].

2.9. Cell viability analysis

C24:0 ceramide (C24 Ceramide (d18:1/24:0) N-lignoceroyl-D-erythro-sphingosine, Avanti Polar Lipids Inc, EE.UU, Alabama) was solubilized in 1 % DMSO and in DMEM media containing 10 % free fatty acid-free Bovine Serum Albumin (Equitech-Bio Inc, EE.UU, Texas) to a final concentration of 5, 10, 15, 20 and 25 μM in 100 μl medium. Then, 3T3-L1, hMSC and HUH7 cells were stimulated with C24:0 ceramide for 24 h and incubated with 150 μM MTT (Cell proliferation kit I, Roche Diagnostics, Mannheim, Germany) during 1 h at 37 °C in a CO2 chamber. Cell viability was quantified at 570 nm wavelength. Results are expressed as percentage of MTT reduction relative to control cells treated with 0.1 % DMSO.

2.10. Quantification of lipid accumulation in 3T3-L1 and the human mesenquimal stem cells (hMSC) and ceramide profiling by lipidomic analysis

Lipid accumulation in 3T3-L1 adipocytes and hMSC (donated by Dr.Koromilas, McHill University, Montreal, Canada) treated with C24:0 ceramide for 14 days was quantified using the oil red solution following manufacturer's instructions. Images were taken in a PrimoVert microscope and an AxioCam ERc5s camera (Zeiss). Oil red stain was quantified at 510 nm using the iMark Microplate Absorbance Reader (Bio-Rad).

Adipocytes differentiated from hMSC were treated with 50uM C24:0 ceramide for 24 h. Following incubation, the medium was removed, and adipocytes were washed twice with 1 ml of PBS. Then lipid extraction was performed using the Bligh & Dyer method [43]. Briefly, adipocytes were dried upside down for 5 min and removed from the culture plate using a mixture of 905uL of water plus 2 mL of methanol (MeOH). This mixture was then transferred to a clean culture glass tube and 900 μL of dichloromethane (DCM) and 50uL of a custom standard mixture of labeled lipids were added to each sample (Avanti UltimateSplash# 330820). The mixture was left for 30 min at room temperature, after which 900uL of DCM and 1 mL of water were added. Then samples were vortexed and

centrifuged at 4600 rpm for 10 min. The organic layer was transferred to a clean glass tube. These steps were done twice to isolate lipids. The pooled organic layers were dried using a LabConco Centrivap at 30 °C for 90min. After drying, samples were reconstituted in 550uL of 10 mM ammonium acetate in DCM:MeOH (50:50).

Lipids were analyzed using a previously published direct injection-differential mobility spectrometry-mass spectrometry method [44]. Ninety microliters of each sample were injected and analyzed via fluid injection (FIA) at a flow rate of 8uL/min using an LC - Exion AD 30. The 6500+ QTRAP (Sciex) platform is equipped with a SelexIon unit, enabling differential mobility separation (DMS). Analysis was conducted using a targeted acquisition list (MRM) with DMS on (Method 1) and DMS off (method 2). Collectively, this allowed for the quantitative measurement of 19 lipid classes, including ceramides. DMS was tuned using EquiSPLASH LIPIDOMIX (Avanti # 330731). Data analysis was performed using the Shotgun Lipidomics Assitant (SLA), a Python-based tool developed by Su et al. [44]. The SLA allows for the customization of lipid and standard Multiple Reaction Monitoring (MRM) transitions and performs isotope corrections, which improve the quantitative accuracy of the data. The data shown herein corresponds to the ceramide profiling of the adipocytes after the stimuli with 50uM of ceramide 18:1/24:0.

2.11. Measurements of mitochondrial respiration, membrane potential (ΔΨm) and mitochondrial Ca2+ content

HUH7 cells were treated with 0, 12.5, 25 and 50 μM of C24:0 for 48h following by sequential addition of oligomycin (2 μM), carbonyl cyanide-p-trifluoromethoxy phenyl-hydrazone (FCCP) (0.5 μM), a mixture of rotenone plus antimycin A (1 μM) and 2-Deoxyglucose (50 mM). Basal, maximal, non-mitochondrial and ATP-linked respiration, proton leak, the spare respiratory capacity and glycolytic and measure oxygen consumption rate (OCR) and extracellular acidification rate (ECAR) were analyzed by Seahorse Extracellular Flux (XF) 96 Analyzer (Agilent Technologies, USA) using the Mito Stress Test Kit. Data were analyzed as described [5].

HUH7 cells, were maintained as described previously and were pre-treated with indicated treatments and then cells were loaded with 1 ml Hank's Balanced Salt Solution (HBSS) pH 7.3–7.4, containing 25 nM TMRM (Thermo fisher, Massachusetts, EEUU) for ΔΨm and 1 μM ER-Tracker Green (Thermo fisher, Massachusetts, EEUU) for 30 min at room temperature (RT). After 30 min cells were washed. Analysis of mitochondrial Ca2+ levels was performed as described previously and cells were loaded with HBSS containing 20 μM Rhod-2 AM (Thermo fisher, Massachusetts, EEUU) and 0.02 % Pluronic F-127 for 30 min at RT. Measurements were acquired using a Zeiss Axiovert 100M confocal microscope with a Plan-Neofluar × 63/1.25 oil immersion objective lens at RT. TMRM fluorescence was excited at 543 nm and ER-Tracker Green excited at 488 nm wavelength laser. Rhod-2, AM fluorescence was excited at 514 nm. Laser power was kept as low as possible to avoid bleaching of the signal. In all experiments, data were collected every 15 s for 12 min.

2.12. Evaluation of endoplasmic reticulum (ER) stress in HUH7 cells

HUH7 cells were treated with 25 μM C24:0 or tunicamycin (Sigma) at a concentration of 1 μg/mL. Tunicamycin is a N-linked glycosylation inhibitor that induces endoplasmic reticulum stress due to accumulation of misfolded proteins in the ER lumen. Cells were collected after 8 or 24 h and lysed in ice-cold RIPA buffer for protein extraction. For protein extraction, cell lysates were mixed in a TissueLyser (Qiagen), incubated on ice for 30 min and centrifuged at 17,400×*g* for 15 min at 4 °C. The supernatant was transferred to a new tube and stored at −80 °C until use. Protein concentration was determined with the Lowry method. Protein samples (40 μg) were separated on a 10 % SDS-polyacrylamide gel and transferred to a polyvinylidene difluoride (PVDF) membranes (Hybond-P, Amersham, GE Healthcare, Chicago, IL, USA) using a wet electroblotting System (Bio-Rad, Hercules, CA, USA). The membranes were blocked for 1 h with 5 % non-fat dry milk and incubated with primary antibodies diluted in blocking solution overnight. Primary antibodies were: eIF2a, JNK, p-eIF2a, p-JNK, CHOP and SREBP-1 (Merck Millipore, Burlington, MA, USA). ATF6, BiP, XBP1, and tubulin (Santa Cruz Biotechnology). Membranes were washed three times with TBS-T for 10 min and then incubated with horseradish peroxidase-conjugated secondary antibody (goat anti-rabbit or rabbit anti-goat) for 1.5 h at RT. Quantification was performed using a chemiluminescent detection reagent (Millipore, MA, USA). Digital images of the membranes were obtained by a ChemiDoc MP densitometer and processed by Image Lab software (Bio-Rad). The results are reported as phosphorylated/total protein ratio. A value of 1 was arbitrarily assigned to the control group, which were used as a reference for the other conditions.

2.13. Statistical analysis

Results were expressed as mean ± standard error of mean. For Western blot statistical analysis, we used ANOVA following post-hoc Tukey test using the program Graphad Prism Version 7. For semiquantitative analysis, we used the ANOVA test followed by Kruskal-Wallis one-way test using Number crunched statistical software (NCSS, LLC, Utah, United States). *$p < 0.05$, **$p < 0.001$. The data sets generated and/or analyzed during the current study, including the lipidomic profile, are available from the corresponding author on reasonable request.

3. Results

3.1. Obese-T2DM subjects display accumulation of C24:0 ceramide in plasma

Fetal programming is a critical determinant in the regulation of energy metabolism throughout life. However, the mechanisms involved in fetal programming-induced metabolic derangements are not fully understood. To identify potential lipid species associated with altered glucose metabolism, we performed a blood lipidomic profile of obese and obese-T2DM subjects to identify potential

lipidomic markers of metabolic disorders. Plasma ceramide profile in obese-T2DM women showed a selective and substantial increase in the C24:0 ceramide but no changes in C16:0, C18:0, C20:0, C22:0, C23:0, and C24:1 species with respect to obese non-diabetic woman (Fig. 1 and 2, Supplementary Fig. 1A). Resembling the profile found in obese-T2DM women, obese-T2DM men showed major accumulation of C24:0 ceramide, but also presented higher levels of C16:0, C22:0 and C24:1 ceramides relative to obese non-diabetic men (Fig. 1B, Supplementary Fig. 1B). Therefore, our present findings identify plasma 24:0 ceramide as a novel lipidic biomarker in a cohort of obese T2DM subjects from México.Fig 3 and 4

3.2. *Fetal programming by CAF diet exposure leads to plasma C24:0 ceramide accumulation in young offspring of rats*

Next, we tested the hypothesis whether exposing dams to a high-energy diet during the fetal stage modulates plasma C24:0 ceramide accumulation in the offspring at early stages of life. We found that fetal programing by feeding F0 females with a CAF diet during the prenatal stage did not change the body weight of the offspring (CAF-Control group) compared with the offspring of dams fed control diet (Fig. 2B). By contrast, offspring switched to CAF after weaning (CAF-CAF group) showed a time-depend significant decrease in body weight with respect to those switched to control (CAF-Control) (Fig. 2B). We also found that exposure to CAF during the fetal period and after weaning (CAF-Control and CAF-CAF groups) promoted fat accumulation in liver, as evidenced by an increase in the number and size of intracellular lipid droplets (Fig. 2C and D). Lipidomic analysis confirmed that CAF exposure before weaning (CAF-Control) significantly increased C23:0, C24:0 and C25:0 ceramide levels in the offspring, whereas maintaining the CAF diet after weaning (CAF-CAF) increased the C16:0, C18:0, C20:0, C22:0, C23:0, C24:0, C24:1 and C25:0 species (Fig. 2E and F). Our data also show that fetal exposure to CAF diet induced significant changes in plasma glycerol species: DG (18:0_18:1, 18:1_16:0, 18:1_18:2, 18:1_18:3) for CAF-Control and CAF-CAF groups when compare to control, respectively (Fig. 2G and H); whereas, an increase of plasma DG (16:0_18:2, 16:0_20:4, 18:1_20:4 and 18:2/18:2) was selectively identified in the CAF-CAF group (Fig. 2G and H). These data give evidence that fetal programming by CAF exposure leads to hepatic steatosis and plasma C24:0 ceramide accumulation in the young offspring.

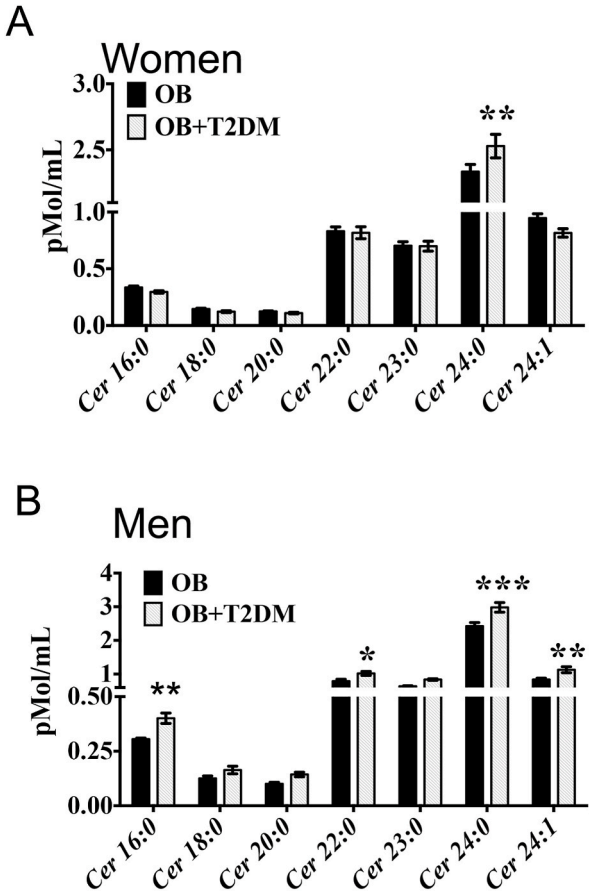

Fig. 1. C24:0 ceramide accumulates in blood samples of male and female obese and obese-T2DM subjects. A-B) Blood samples were collected from female obese (n = 40) or obese-diabetic (n = 34) and male obese (n = 20) or obese-diabetic subjects (n = 18) as described Materials and Methods. Plasma concentrations were determined by quantitative tandem mass spectrometry. Data are expressed as mean ± SEM. *$p < 0.05$, **$p < 0.001$, ***$p < 0.0001$ of obese-T2DM vs. obese following ANOVA and post-hoc Tukey′s test. Abbreviations, OB: Obese; T2DM: Type 2 diabetes Mellitus.

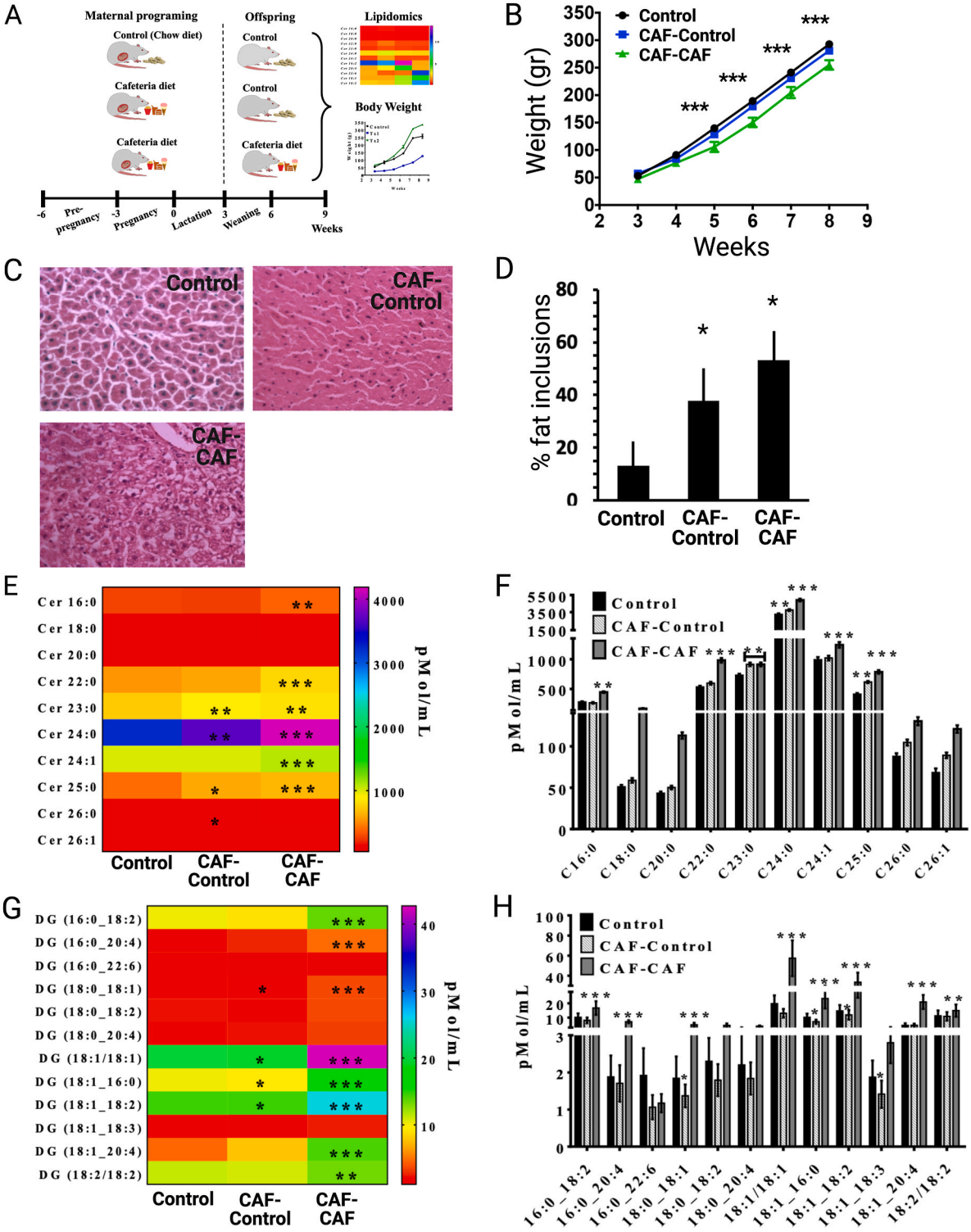

Fig. 2. Fetal programming by CAF diet accumulates plasma C24:0 ceramide in offspring of rats. A) Maternal nutritional programing was performed by exposing mothers (n = 10) to *ad libitum* control chow diet (Control group, n = 4), or CAF diet (CAF group, n = 6) for 9 weeks (pre-pregnancy, pregnancy and lactation). After weaning (21st postnatal day) males offspring from mothers exposed to Chow or CAF diets were allocated into three experimental groups (n = 10–12 each): the control Chow group kept the Chow diet exposure (Control, group), and CAF group was exposed to Chow diet (CAF-Control group) or CAF diet (CAF-CAF group). B) Body weight changes after weaning for Control, CAF-Control and CAF-CAF groups (***p < 0.0001 CAF-CAF vs Control). C, D) Histological assessment of liver of Control, CAF-Control and CAF-CAF groups and percentage of lipid inclusions

(*p < 0.05 CAF-CAF, CAF-Control vs Control). Heatmap and graph of plasma ceramides (E, F) or diacylglycerols (G, H) profile concentrations in offspring. Plasma concentrations were determined by quantitative tandem mass spectrometry as described in Materials and Methods (*p < 0.05, **p < 0.001, ***p < 0.0001 CAF-CAF or CAF-Control vs Control). All data are expressed as mean ± SEM following ANOVA and post-hoc Tukey 's test. *p < 0.05, **p < 0.01, ***p < 0.001.

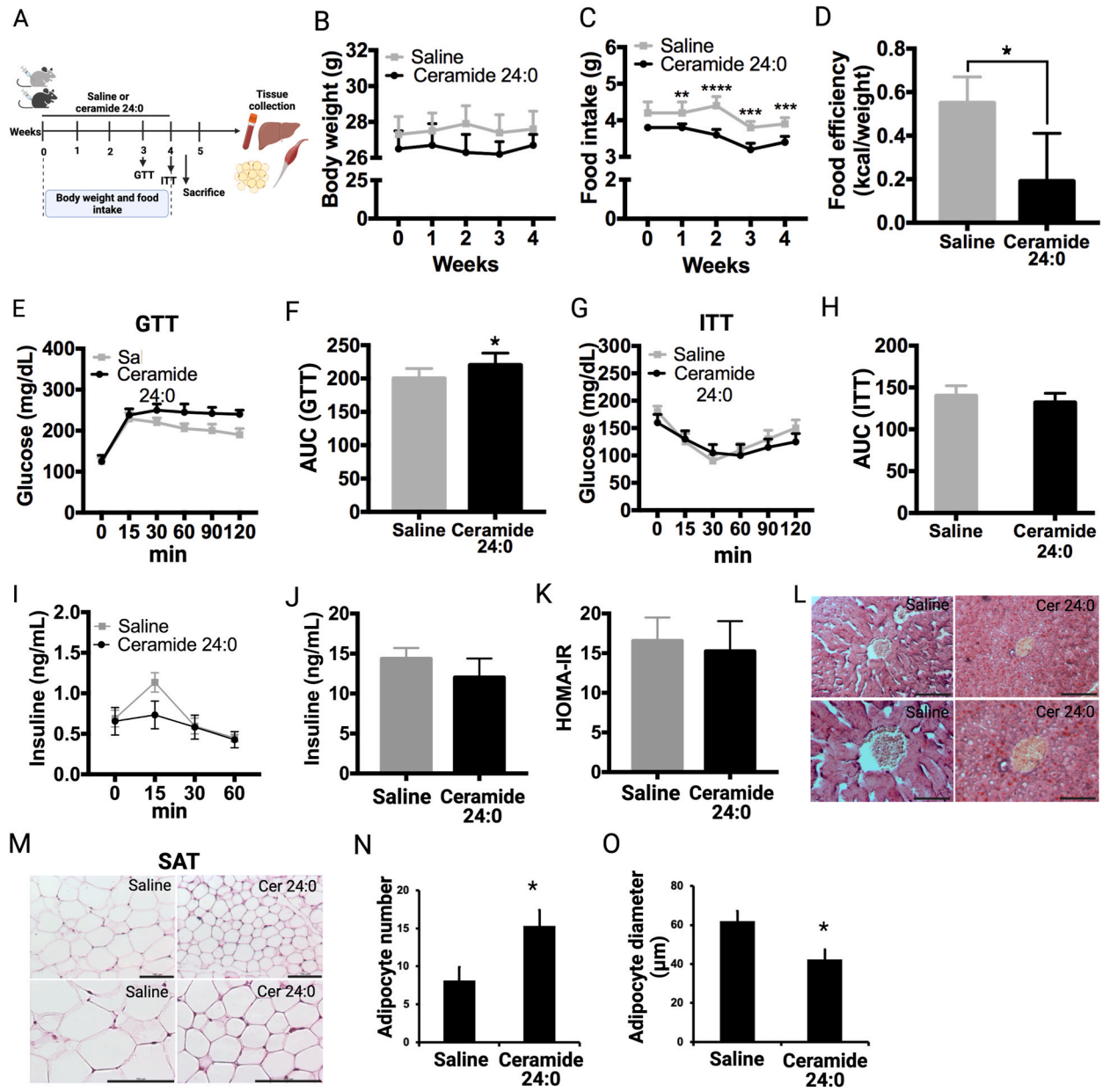

Fig. 3. Effect of chronic C24:0 ceramide administration on weight, food intake and glucose balance in mice. A) Experimental design of chronic C24:0 ceramide administration in mice on glucose homeostasis. Mice were i.p. administered with 3.5 nmol/ml C24:0 ceramide (n = 12) or saline (n = 10) in 100 µL for 4 weeks. GTT (B,C) and ITT (D,E) were performed at 15, 30, 45, 60, 90, and 120 min and AUC is shown. Insulin levels in mice exposed to during the GTT test were quantified 3.5 nmol/ml C24:0 ceramide or saline were quantified (F,G) and HOMA-IR index was determined (H). Hematoxilin and Eosin staining of the liver (I) and SAT (J) was performed. Adipocyte number (K) and adipocyte diameter (L) were quantified from SAT. Bar = 200 µm. Data show the normalized results of mean ± SEM and statistical significance after using ANOVA following by post-hoc Tukey test for body weight, food intake, GTT, ITT test and "t" student for food efficiency. *p < 0.05, **p < 0.001, **p < 0.0001. Abbreviations, AUC: Area Under Curve; SAT: Subcutaneous adipose tissue.

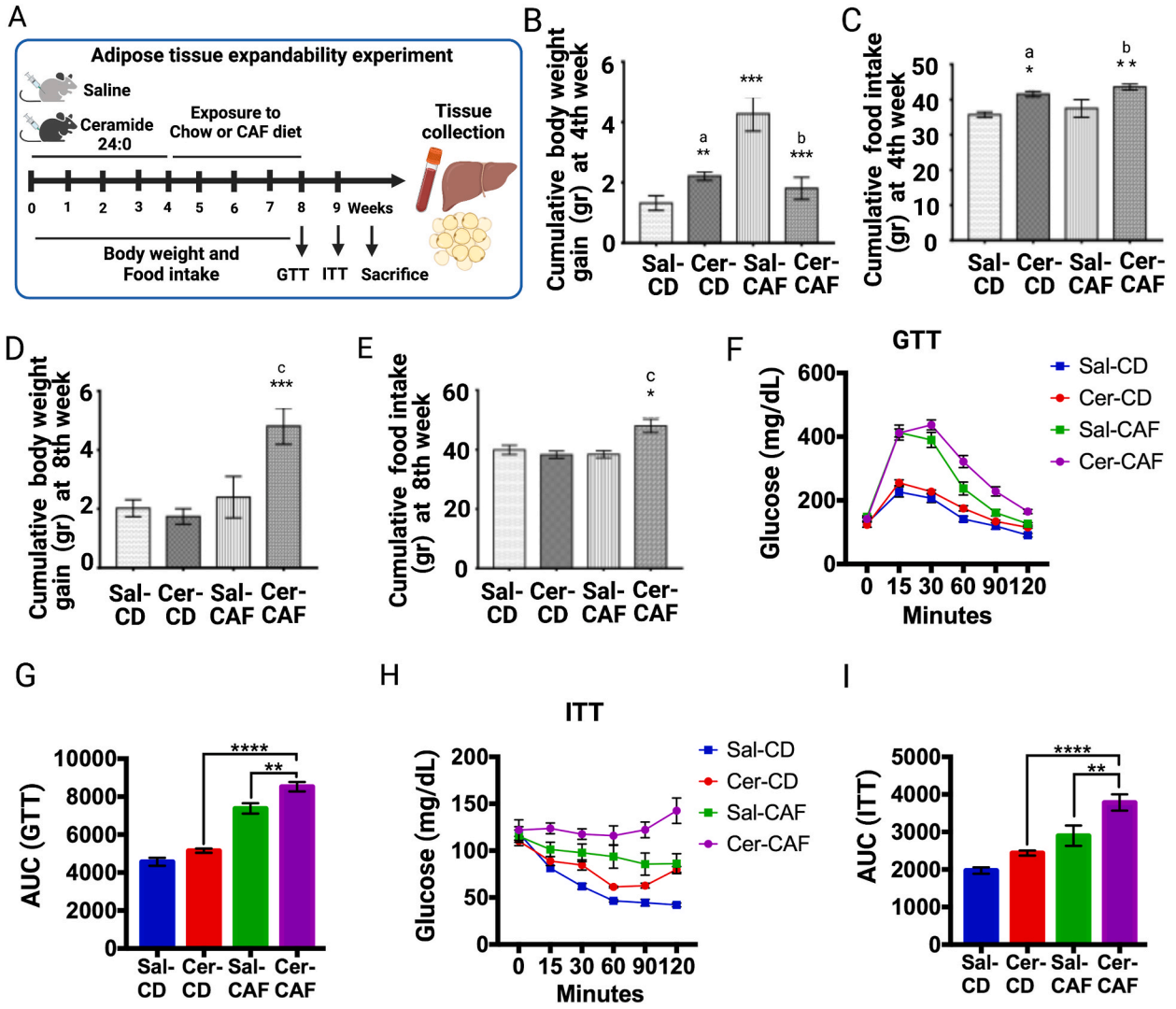

Fig. 4. Effect of chronic C24:0 ceramide administration on glucose balance and adipose tissue expandability followed a CAF challenge. A) C57BL/6 mice were chronically treated with C24:0 ceramide (3.5 nmol/ml) C24:0 ceramide (n = 24) or saline (n = 20) in 100 μL for 4 weeks and exposed to Chow (n = 12 per group) or CAF (n = 10 per group) diet for 4 weeks. Food and body weight were recorded daily, and GTT and ITT assessments were evaluated at 7th and 8th weeks, respectively. Cumulative body weight (B) and Food intake (C) at 4th week and Cumulative body weight (D) and Food intake (E) at 8th week were recorded. GTT (F,G) and ITT (H,I) were performed at 15, 30, 45, 60, 90, and 120 min and AUC is shown. Data show the normalized results of mean ± SEM and statistical significance after using ANOVA following by post-hoc Tukey test for body weight, food intake, GTT, ITT test and "t" student for food efficiency. *p < 0.05, **p < 0.01, ***p < 0.001. [a] vs Sal-CD, [b] vs Sal-CAF, [c] vs Sal-CD. Abbreviations, CD: Control diet; Sal: Saline; Cer: ceramide; CAF: Cafeteria.

3.3. C24:0 ceramide promotes hyperphagia, glucose metabolism imbalance and defective WAT remodeling

Ceramides have been identified as a selective trigger of metabolic disorders by its detrimental effects on glucose homeostasis, insulin sensitivity and fatty acids metabolism [14]. Each ceramide species exerts distinct effects depending on chain length, the presence of double bonds and their accumulation in selective body organs. However, the role of fetal programming on plasma ceramides accumulation in the offspring that leads to glucose imbalance and T2DM susceptibility, have not been characterized. Here, we administered mice with daily intraperitoneal injections of C24:0 ceramide-FAF-BSA (3.5 nmol/ml) or saline-FAF-BSA for 4 weeks to evaluate its impact on body weight and glucose metabolism. We found that chronic C24:0 ceramide injection for 4 weeks increased plasma glucose concentrations during the ipGTT (Fig. 3B and C), while no differences were observed in the glucose curve during the ITT (Fig. 3D and E), indicating that the reduction in glucose tolerance in mice administered C24:0 is not primarily due to impaired insulin signaling. To evaluate if the lack of correlation between GTT and ITT results were due to differences in insulin secretion, we evaluated circulating insulin during the GTT. Remarkably, mice administered with C24:0 ceramide did not affect insulin concentrations in response to the glucose challenge (Fig. 3F and G) nor HOMA-IR (Fig. 3H) in response to C24:0 ceramide. These results reveal

that chronic C24:0 ceramide exposure disrupts physiological glucose homeostasis.

One of the main activities of adipose tissue is to store surplus energy as triglycerides to avoid lipid overaccumulation in other tissues, preventing lipotoxicity. Accordingly, a reduction in insulin sensitivity or secretion can increase adipose tissue lipolysis and lipid accumulation in peripheral tissues. We found that administering mice with C24:0 ceramide for 4 weeks increased hepatic fat content, as assessed by oil red O staining (Fig. 3I), and decrease subcutaneous adipocyte diameter in the SAT, reflected as a greater number of adipocytes per quadrant (Fig. 3J, K, L). These results suggest that chronic C24:0 ceramide exposure disrupts physiological glucose homeostasis and increasing basal lipolysis in SAT. These alterations potentially might favor excessive lipid accumulation in liver along with insufficient insulin-mediated suppression of hepatic glucose production.

An early event leading to adipose tissue dysfunction during obesity is impaired expansion capacity. A positive energy balance forces adipose tissue to expand in order to increase its lipid storage capacity. This expansion occur by increasing adipocyte size (hypertrophy) and/or adipocyte number (hyperplasia) [29]. However, the inability of adipose tissue to efficiently increase hyperplasia leads to an accumulation of hypertrophic adipocytes. This dysfunctional adipocytes are characterized by increased basal lipolysis, which lead to fat accumulation in non-adipose organs, causing metabolic alterations [29]. Based on our previous results, we tested the hypothesis that the impaired adipose tissue expandability trough C24:0 ceramide injection would make animals more susceptible to a high-energy diet challenge. For this purpose, mice were administered C24:0 ceramide-FAF-BSA or Saline-FAF-BSA for 4 weeks as described previously and then fed a control Chow or CAF diet for an additional 4 weeks (Fig. 4A). We found that after 4th week, C24:0 ceramide administration increased body weight gain and food intake in mice fed the Chow diet compared to those administered saline (Fig. 4B

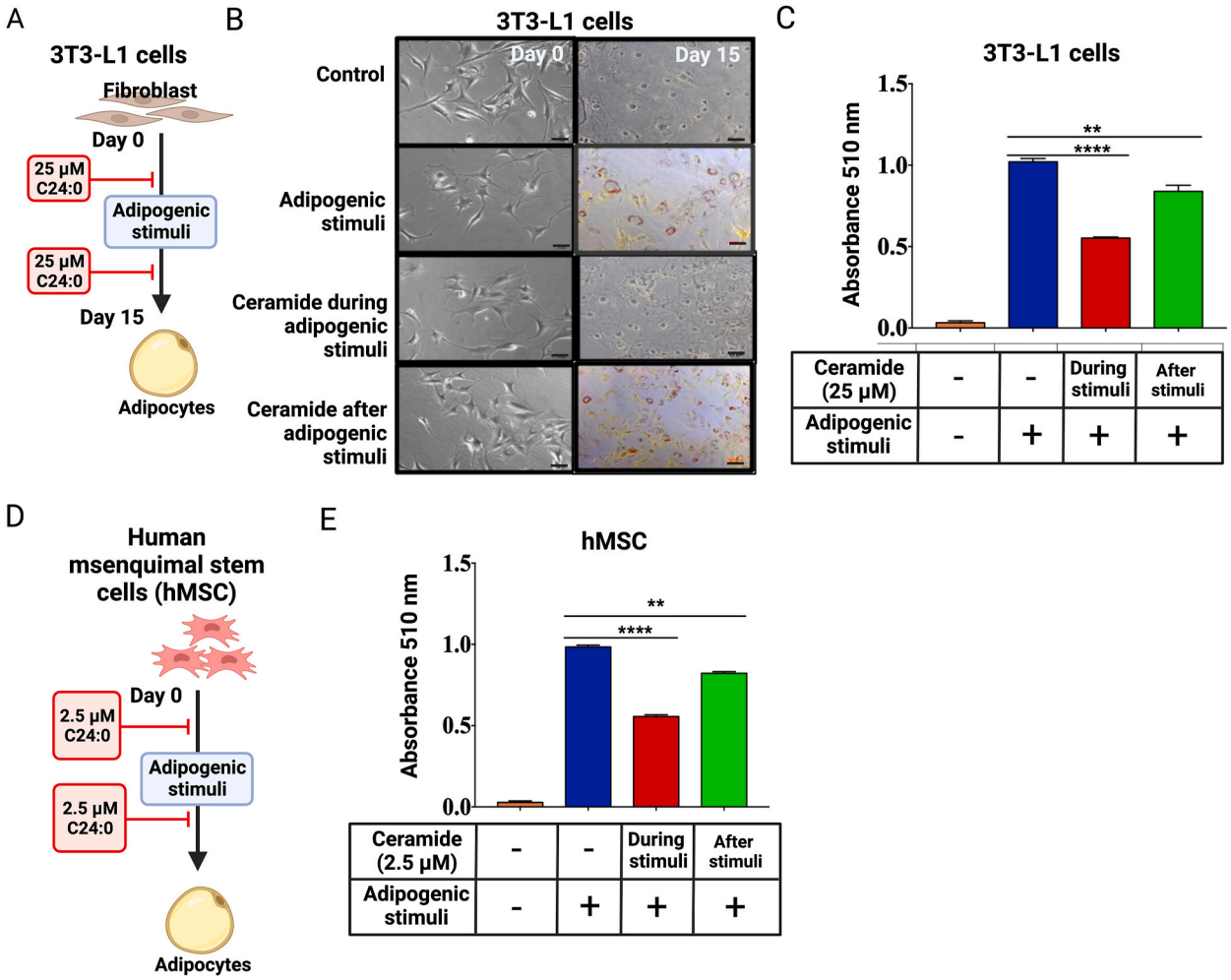

Fig. 5. Adipogenic differentiation of 3T3-L1 cell line and hMSC is impaired during C24:0 ceramide stimulation. A) 3T3-L1 or hMSC (D) cells were maintained in DMEM-high glucose + 10 % newborn calf serum, as described. Cells were 25 µM C24:0 ceramide-10 % FFA-BSA incubated before and after adipocyte differentiation by adipogenic stimuli for 11 days or 14 days, respectively. For control 1 % DMSO was added to a final concentration. Cellular lipid accumulation in 3T3-L1 (B, C) or hMSC (E) was conducted by adding oil red O solution following manufacturer's instructions and measured at 510 nm. Graphs show the normalized results of mean ± SEM for n = 3–4 independent experiments and statistical significance after using ANOVA following by post-hoc Tukey test. **p < 0.01, ***p < 0.001.

and C). Also, at 8 weeks, mice fed CAF diet and exposed to C24:0 ceramide showed increased cumulative body weight gain and food intake compared to the other groups (Fig. 4D and E). Accordingly, the ipGTT and ipITT revealed that C24:0 ceramide induced glucose intolerance and insulin resistance, respectively in mice fed the CAF diet when compared with mice fed Chow control diet or mice administered with saline (Fig. 4F–I). Together, these results confirm that C24:0 ceramide primes body weight gain, glucose imbalance and adipose tissue dysfunction in mice exposed to a high-energy diet challenge.

3.4. C24:0 ceramide block adipogenic differentiation in the 3T3-L1 cell line and hMSC

To gain insight into the mechanisms involved in the deleterious effect of C24:0 ceramide in adipocyte hyperplasia, we assessed the effect of C24:0 ceramide on adipocyte differentiation capacity using the adipogenic cell line 3T3-L1 and hMSCs (Fig. 5A–D). Exposing adipocytes to C24:0 ceramide-FAF-BSA for 24 h showed a time and dose-dependent effect on cell toxicity, where 3T3L1 adipocytes-maintained viability at ceramide concentrations as high as 25 μM (Supplementary Fig. 2A). However, incubating hMSC cells during the 14 days of adipogenic differentiation robustly decreased cell viability. No changes were found at 2.5 μM C24:0 (Supplementary Fig. 2C). We then exposed 3T3-L1 and hMSC to 2.5 μM or 25 μM C24:0 ceramide respectively during or after adipogenic stimuli (Fig. 5A–D). We found that 25 μM C24:0 ceramide incubation during adipogenic stimuli reduced lipid droplets formation, as evidenced by a decrease in oil red O staining (Fig. 5B and C). Strikingly, exposure to C24:0 ceramide after adipogenesis also blocked lipid droplets formation of mature adipocytes in both 3T3-L1 (Fig. 5B and C) and hMSC (Fig. 5 E) cells. These results confirm the detrimental effect of C24:0 ceramide on adipocyte differentiation and lipid accumulation capacity.

Finally, to determine if C24:0 ceramide can be taken up and metabolized by adipocytes, we incubated hMSC-derived adipocytes with 50 μM C24:0 ceramide for 24 h. Then, total lipids were extracted and subjected to LC-ESI-MS/MS to measure individual lipid

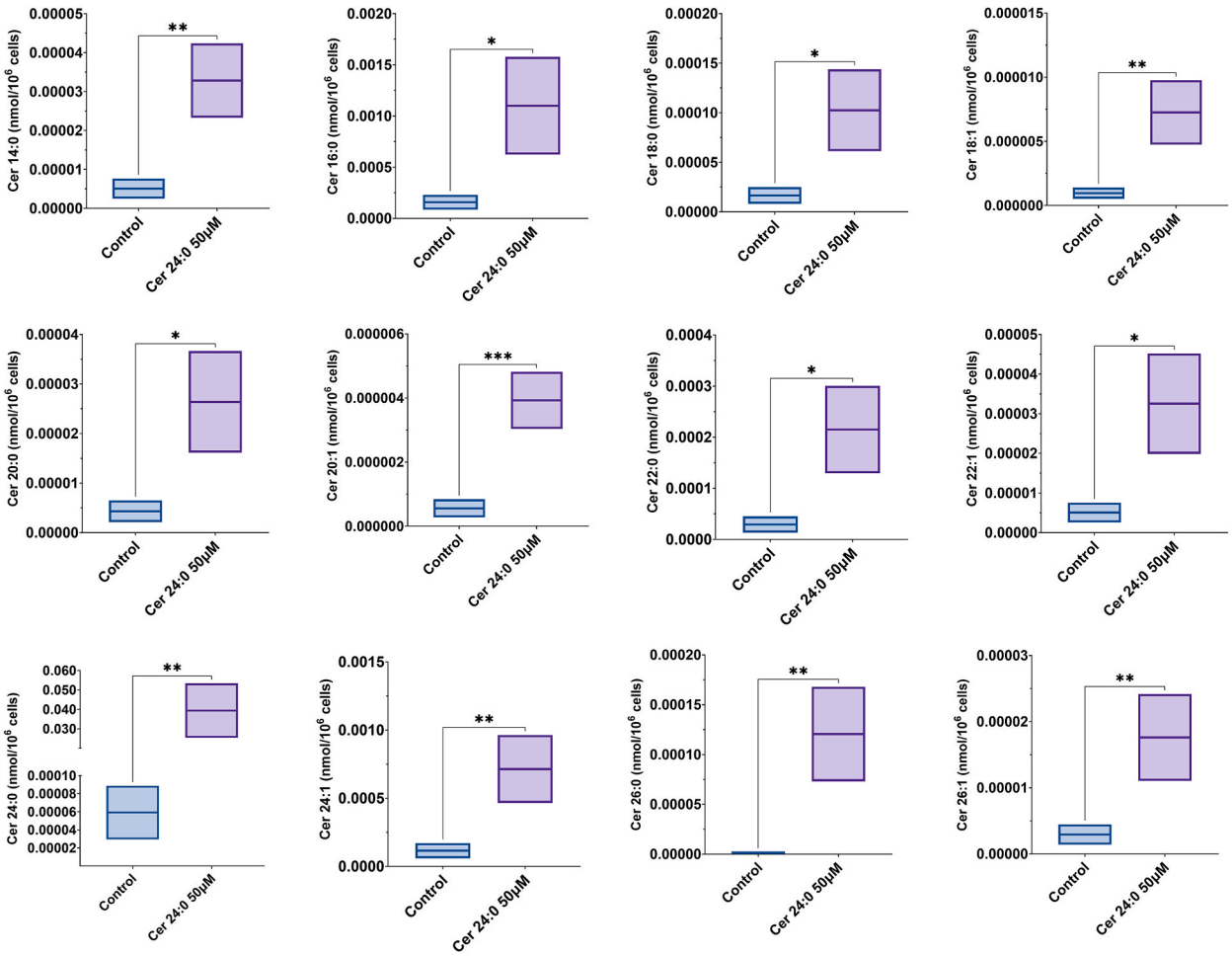

Fig. 6. Boxplots showing the distribution of twelve distinct ceramide species (Cer 14:0, Cer 16:0, Cer 18:0, Cer 18:1, Cer 20:0, Cer 22:0, Cer 22:1, Cer 24:0, Cer 24:1, Cer 25:0, Cer 26:0, and Cer 26:1) detected by DMS mass spectrometry in control and Cer 24:0 50 μM-treated groups. Significant differences in ceramide levels between the groups are indicated by asterisks ($P < 0.05$, $^{**}P < 0.01$, $^{**}P < 0.001$). The treatment with Cer 24:0 50 μM led to noticeable increases in various ceramides compared to the control group.

species. Lipidomic analysis revealed that adipocytes incubated with the C24:0 ceramide accumulated the C24:0 specie, but also many other ceramide species such as C14:0, C16:0, C18:1, C20:1, C22:0, C22:1, C24:1, C26:0 and C26:1 (Fig. 6). These results imply that adipocytes possess the machinery needed to uptake ceramide and modify it by increasing or decreasing fatty acid chain length and unsaturation.

3.5. C24:0 ceramide impairs mitochondrial energetics, decreases ΔΨm and augments mitochondrial calcium overload in HUH7 cells

C16:0 and C18:0 ceramide species have been reported to disrupt mitochondria function in mice [17,21,22] and mitochondrial dysfunction is an early alteration in the development of Metabolic Dysfunction-Associated Steatotic Liver Disease (MASLD) [45]. Thus, to evaluate whether ceramide-dependent hepatic lipid accumulation involves the disruption in mitochondrial bioenergetics, we tested whether exogenous very long acyl chain C24:0 ceramide disrupts mitochondrial function in hepatic cells. We first evaluated the dose-dependent effect of C24:0 ceramide on HUH7 cells viability. As observed in the 3T3-L1 cells, 5–25 μM C24:0 ceramide does not affect viability in the HUH7 cells (Supplementary Fig. 2B). We then, measured mitochondrial bioenergetics as well as glycolysis by a time-dependent oxygen consumption rate (OCR) and extracellular acidification rate (ECAR) in HUH7 cells exposed to a different range of C24:0 ceramide concentrations. Ceramide C24:0 incubation promoted a dose-dependent decrease in ECAR during the oligomycin, FCCP and rotenone stimulation when compared with control (Fig. 7A). Also, we found a dose-dependent reduction of the glycolytic reserve during C24:0 ceramide incubation (Fig. 7B), which was associated with a decrease in fatty acid utilization (Fig. 7C). Additionally, C24:0 incubation decreased basal respiration, OCR associated to ATP-production, H+ leak, maximal respiration, spare respiratory capacity and non-mitochondrial respiration denoting impaired mitochondrial respiration (Fig. 7D and E). These results indicate that ceramide C24:0 affects mitochondrial activity decreasing its oxidative capacity and therefore promoting fatty acid accumulation in HUH7 cells.

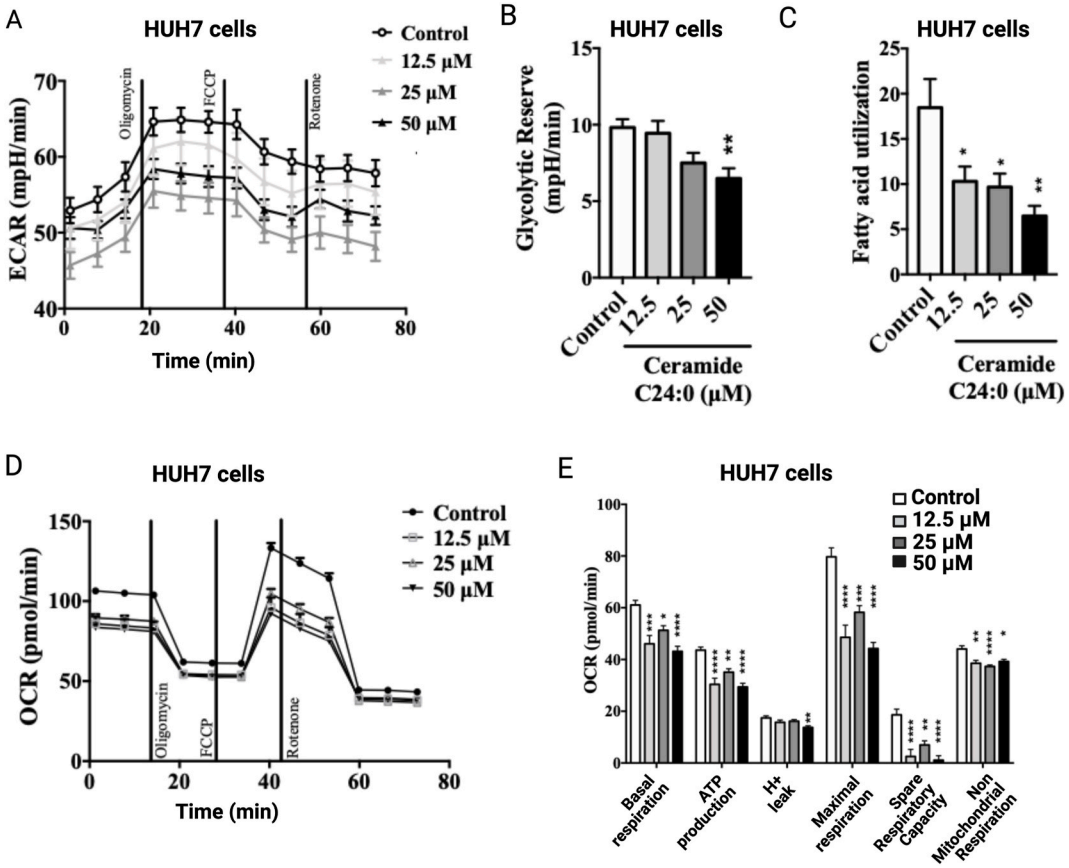

Fig. 7. Cer 24:0 ceramide disrupts mitochondrial oxygen consumption and fatty acid utilization in HUH7 cells. Cells were treated with 12.5, 25, or 50 μM C24:0 ceramide-10 % FFA-BSA for 80 min and ECAR (A), Glycolytic Reverse (B), fatty acid utilization (C), OCR (D) or OCR H+ leak, maximal respiration, spare respiratory capacity and non-mitochondrial respiration (E) were determined using Seahorse technology. Data show the normalized results of mean ± SEM for n = 3–4 independent experiments and statistical significance after using ANOVA following by post-hoc Tukey test. *p < 0.05, **p < 0.01, ***p < 0.001 vs Control. Abbreviations, OCR: Oxygen consumption rate; ECAR: extracellular acidification rate.

3.6. C24:0 ceramide disrupted mitochondrial function, decreased ΔΨm and favored mitochondrial calcium overload in HUH7 cells and in adipocytes from mice fed a high-energy diet

To evaluate the effect of C24: 0 ceramide on mitochondrial electrochemical gradient and calcium homeostasis, HUH7 cells were loaded with TMRE to measure changes in ΔΨm using confocal microscopy. As expected, C24:0 ceramide decreased the ΔΨm in a time-dependent manner. The inhibitory effect was evident immediately after 1h of incubation and remained for 3h (Fig. 8A and B). Notably, 3h C24:0 ceramide incubation also induced calcium overflow into the mitochondrial matrix, evidenced by enhanced Rhod-2 AM signal (Fig. 8C and D).

Finally, we tested whether adipose tissue of mice treated with C24:0 ceramide and exposed to high-energy diets integrates impairment in mitochondria function (Fig. 8E). We found that adipocytes isolated from SAT of mice inoculated with C24:0 ceramide

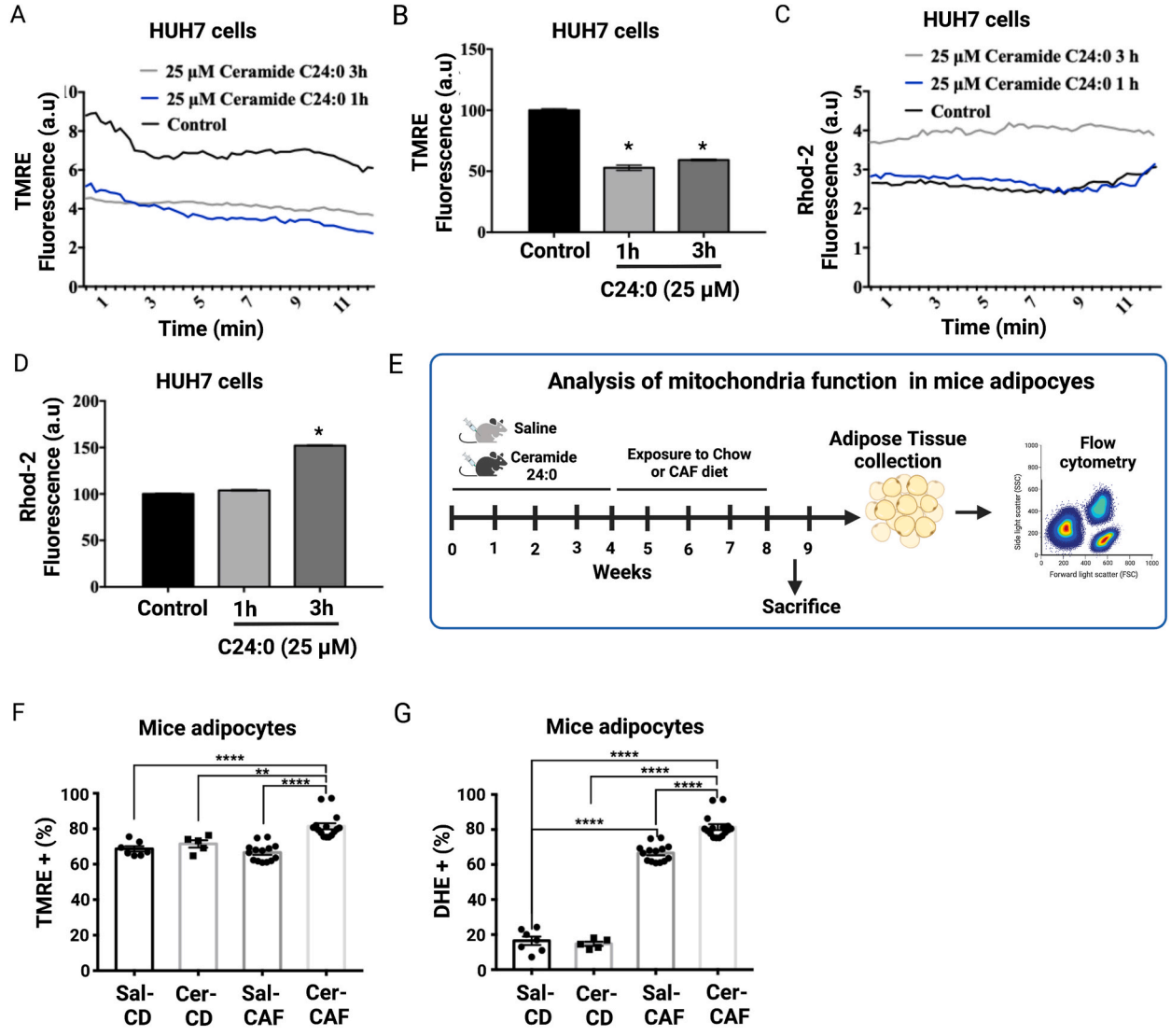

Fig. 8. Cer 24:0 ceramide promotes mitochondrial calcium overload and mitochondria membrane potential depolarization in HUH7 cell and mice adipocytes. HUH7 cells were treated with 25 µM C24:0 ceramide-10 % FFA-BSA for 1 or 3h and mitochondrial and ER dysfunction and mitochondrial calcium were determined using TMRE (A, B) or Rhod-2 AM (C,D) trackers and confocal microscopy, respectively. Data show the normalized results of mean ± SEM for n = 3–4 independent experiments and statistical significance after using ANOVA following by post-hoc Tukey test. *p < 0.05, **p < 0.01, ***p < 0.001. E) Mouse SAT was isolated as described [42], and cells were stained with BODIPY (2 µM) TMRE (100 nM) or DHE (1 µM) and incubated for 30 min at 37 °C. Mitochondrial membrane potential (F) and ROS production (G) were determined by flow cytometry (BD Accuri C6) using the FL1 for BODIPY+ and the FL3 channel for TMRE + or DHE+. All of the events that were positive for the FL1 channel were considered as adipocytes and that is where we measured the loss of mitochondrial potential or ROS production using the BD Accuri C6 software. Data show the normalized results of mean ± SEM for n = 6–8 mice per group and statistical significance after using ANOVA following by post-hoc Tukey test. *p < 0.05, **p < 0.01, ***p < 0.001, ****p < 0.0001.

and exposed to a high-energy diet challenge (CAF diet) showed loss of the mitochondria membrane potential (Fig. 8F), which correlates with an increased in ROS production (Fig. 8G), when compared to mice treated with saline. Also, we found an increased in ROS production in mice treated chronically with saline and exposed to CAF diet (Fig. 8G). These *in vitro* and *in vivo* results confirm that the C24:0 ceramide clearly disrupts mitochondrial function, promoting mitochondrial calcium overload and ROS generation, and disrupts

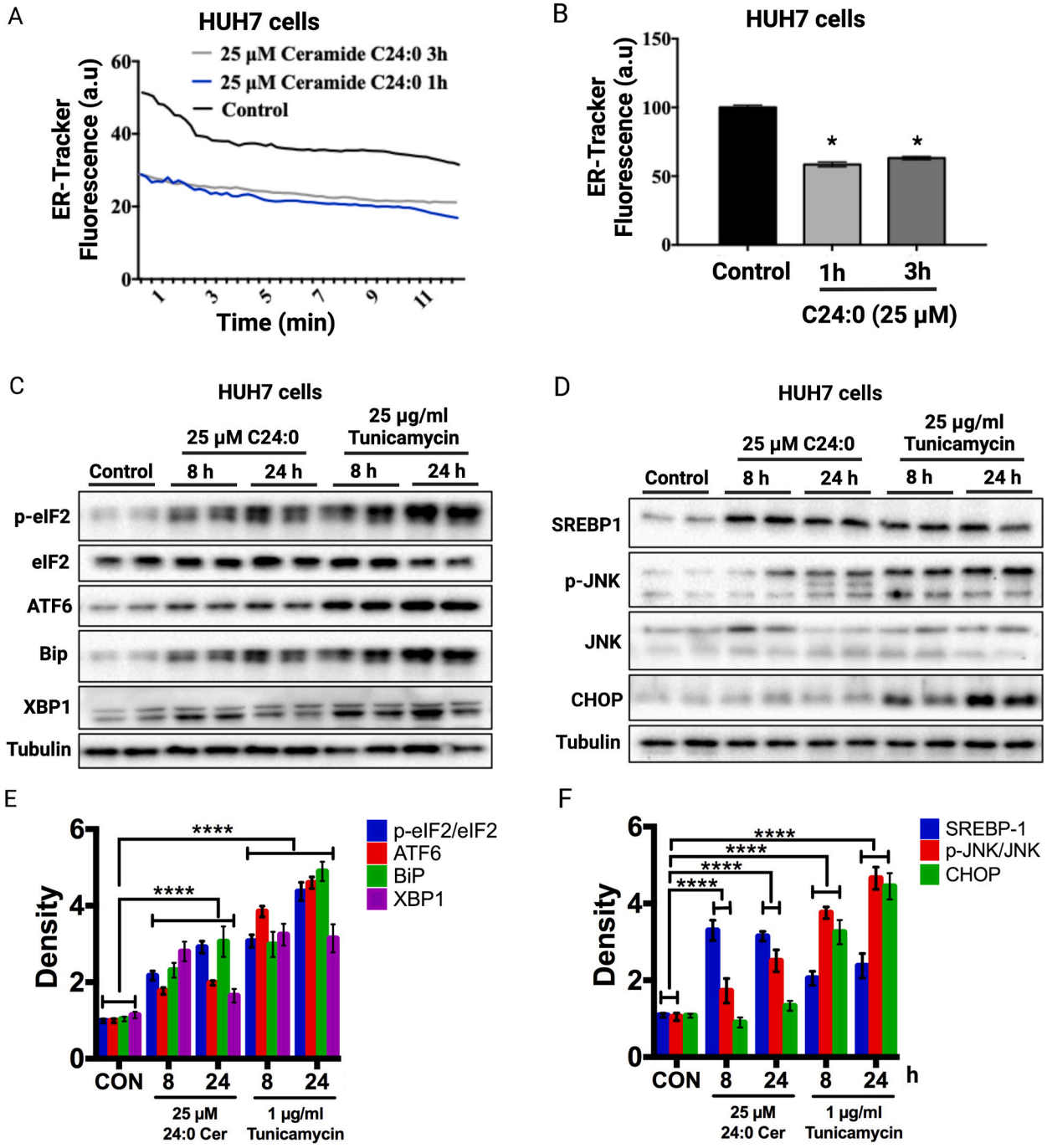

Fig. 9. Cer 24:0 ceramide promotes ER stress in HUH7. Cells were treated with 25 μM C24:0 ceramide-10 % FFA-BSA for 1 or 3h and ER dysfunction was determined using ER-Tracker Green (A, B) trackers and confocal microscopy, respectively. Data show the normalized results of mean ± SEM for n = 3 independent experiments and statistical significance after using ANOVA following by post-hoc Tukey test. *p < 0.05, **p < 0.001, ***p < 0.0001. HUH7 cells were incubated with 25 μM C24:0 ceramide-10 % FFA-BSA or 25 μg/ml tunicamycin for 8 or 24 h and Western blot against p-eIF2/ATF6, ATF6, Bip or XBP1 (C, E) or SREBP1, p-JNK/JNK or CHOP (D, F) were performed. Data show the normalized results of mean ± SEM for n = 3 independent experiments and statistical significance after using ANOVA following post-hoc Tukey test. *p < 0.05, ****p < 0.0001.

adipose tissue function to the effects of a high-energy diets challenges.

3.7. C24:0 induces endoplasmic reticulum stress and SREBP1 proteolytic activation in HUH7 cells

To gain insight into the mechanisms trough which C24:0 ceramide induces mitochondrial dysfunction, we evaluated endoplasmic reticulum (ER) stress markers in HUH cells. ER stress is a cellular response to diverse insults in the ER lumen, including the accumulation of unfolded proteins, lipid and glucose buildup, oxidative stress and alterations in Ca + homeostasis. Recent evidence has highlighted the role of ER stress in the development of mitochondrial dysfunction and the involvement of sphingolipids, such as ceramide in this degenerative process [46]. ER stress activates a signaling pathway known as unfolded protein response (UPR) consisting in three signaling branches: the PERK, ATF6 and IRE1 pathways [47]. We first analyzed the ER response to C24:0 ceramide in HUH7 cells by loading them with the ER-tracker green and then visualizing using confocal microscopy. We found a decrease in the ER-tracker signal followed C24:0 ceramide incubation at 1h and 3h, indicating a perturbation in ER integrity (Fig. 9A and B). To determine if C24:0 ceramide induces ER stress in hepatocytes, we incubated HUH7 cells in the presence of 25 μM C24:0 ceramide or 1 μg/ml of the protein glycosylation-inhibitor tunicamycin for 8 or 24 h and evaluated several UPR markers by Western blot. We found that C24:0 ceramide induced a time-dependent increase in UPR markers p-eIF2, ATF6, BiP and XBP1 but at a lesser extent than tunicamycin (Fig. 9C–E). Interestingly, C24:0 ceramide increased the content of the mature form of the lipogenic transcription factor SREBP1 and the phosphorylation of JNK (Fig. 9D–F). Unexpectedly, C24:0 did not increase CHOP protein abundance as observed with tunicamycin (Fig. 9D–F). Finally, C24:0-mediated JNK activation but not CHOP indicates that this ceramide induces cellular inflammation but not enough to induce apoptosis (Fig. 9D–F). These results indicate that C24:0 ceramide disrupts the ER membrane, activating the UPR and inflammatory signal activation, thereby promoting mitochondrial dysfunction.

4. Discussion

Obesity and maternal over nutrition during pregnancy lead to metabolic disorders in the offspring that prime chronic-related diseases in later life, including T2MD [2]. Here, we identified that fetal programming by CAF diet exposure increases plasma C24:0 ceramide levels in male mice, a lipid specie also found accumulated in blood samples of a Mexican cohort of obese-T2DM subjects. Biological characterization confirmed that C24:0 ceramide impairs adipocyte differentiation and lipid accumulation in 3T3-L1 and hMSC cells, and disrupts mitochondria membrane potential, oxygen consumption and beta oxidation which correlates with excessive mitochondria calcium influx in hepatic HUH7 cells, and in adipocytes from murine models. C24:0 ceramide also induced ER stress, activating the UPR, leading to activation of lipogenic and inflammatory pathways in hepatocytes. *In vivo* data confirm that systemic C24:0 ceramide administration induces glucose intolerance and promoted liver steatosis and decreased adipocyte size during a high-energy diet challenge. We propose that fetal programming by high-energy diets primes plasma C24:0 ceramide accumulation in the offspring which contribute to early glucose imbalance, liver steatosis and failure in adipocyte remodeling followed a high-energy diet challenge.

Ceramides have been reported to negatively affect metabolic nodes related to glucose balance and insulin-related pathways [14,18,19]. In the current study, we characterized plasma ceramide profile in obese and obese-T2DM subjects in a Mexican cohort showing accumulation of C16:0, C18:0, C20:0 and C22:0 species, pointing to the C24:0 ceramide as the major lipid specie found in obese-T2DM subjects. The C24:0 ceramide is the most abundant lipid specie reported in human plasma [48], whereas lysophosphatidylcholines, MHC 24:0, Cer 18:0 and dCer24:1 ceramides and long-chain fatty-acid-containing dihydroceramides have been also determined in plasma of obese and/or obese-T2DM individuals [14,49–52]. Decrease in plasma C14:0 ceramide improves insulin sensitivity [52], in a C14:0 or C18:0-dependent relationship [52,53], which it also depends on ethnicity [54]. Supporting what we found in our study, C24:0 ceramide accumulation was identified in a Mexican American cohort [55], and a high-energy diet overfeeding increases it even further [50], as we found in our murine model. A current limitation of our study indicates lacking lipidomic profile in a normal weight human cohort to be compared with obese and obese/diabetic subjects.

One of the major strengths of our study confirmed major accumulation of plasma C24:0 ceramide in the offspring of mice exposed to high-energy diets during fetal programming. Previous reports documented increased in body weight followed exposure to high-fat diets [56,57] and greater fat accumulation and glucose intolerance in offspring on a nutritional programming schedule [5,9,56,57], which seems to behave in a sex-dependent manner [8,10]. Biological assessment of the effect of C24:0 ceramide on metabolic disruption in naïve mice resembled what we found in the fetal programming model [5], confirming fat accumulation and glucose intolerance [5]. Perhaps a current caveat of this study is to clarify the C24:0 ceramide source during fetal programming. A recent report confirms that a consumption of a high-fat diet increased the accumulation of C14:0, C16:0, C18:0, C20:0, C22:0 and C24:0 ceramides in intestinal enterocytes (https://www.science.org/doi/epdf/10.1126/sciadv.adp2254). Notably, C14:0 and C16:0 ceramides are blood transported and deliver by chylomicrons (https://www.science.org/doi/epdf/10.1126/sciadv.adp2254). No clear evidence has been reported documented the C24:0 ceramide source during fetal programming. Our data suggest that the prenatal programming by high-energy diets set a lipotoxic priming of C24:0 ceramide accumulation in plasma which might target and disrupt insulin-depended metabolic settings at early stages of postnatal life.

A second major contribution of this study confirmed that naïve mice treated with C24:0 ceramide decreased SAT size. It is expected that exposure to high-fat diets accumulates lipids into the WAT which experiences expandability by increasing size (hypertrophy) and/or by number (hyperplasia) of adipocytes [29]. Mechanistically, hyperplasia of WAT maintains glucose metabolism and prevents T2DM, independently from total fat mass [29]. Accordingly, fetal programming by high-fat diet exposure have confirmed SAT hypertrophy in male offspring [58]. Ceramides accumulation into SAT depots followed exposure to a high fat diet [59], such as C16:0 and

C:18 species, might induce adipose tissue inflammation and alterations in glucose metabolism [17,19,60,61], no clear evidence have been documented. In the current study, we did not characterize the lipidomic profile in the SAT of mice chronically treated with C24:0 ceramide and exposed to high-energy diets, which integrates a potential limitation to propose causality for defective adipose tissue remodeling. A recent report provides a clue of the effect of prenatal programming by high-energy diets on WAT lipidomic changes by showing no major changes in triglyceride lipid species [10]. Together, our data clearly indicates that the C24:0 ceramide specie in the offspring actively impaired adipose tissue size during a high-energy diet challenge favoring glucose intolerance.

We used 3T3-L1 and hMSCs cellular models to dissect potential molecular mechanism involved in adipose tissue function during C24:0 ceramide stimulation. We identified that chronic C24:0 incubation to 3T3-L1 and hMSCs impaired adipocyte differentiation hindering lipid accumulation. Also, we found that hMSC-derived adipocytes incorporate C24:0 ceramide leading to C14:0, C16:0, C18:1, C20:1, C22:0, C22:1, C24:1, C26:0 and C26:1 synthesis. Characterization of long chain and unsaturation ceramides biosynthetic enzymes in adipose tissue has not been totally described. Depending on the acyl chain length, six different ceramide synthases (CerS1-6) most commonly produce ceramides ranging from 14 to 26 carbons (C14-C26) [62]. A potential scenario suggests that C24:0 ceramides and new C24:0 ceramide-derived lipid species are produced by selective ceramide enzymes affecting adipose tissue function, while causing a range of adverse consequences associated with obesity. Recent reports have identified that C2DhCer [63] or C6-ceramide [64] treatment in 3T3-L1 cells or murine mesenchymal stem cells, respectively, hampers adipocyte differentiation. Molecularly, C2DhCer or C6-ceramide decreases the adipogenic gene expression program, including AP2, LPL, PLN1 and GLUT4 regulated by PPARgamma2 [63,64], suggesting that C24:0 ceramide or C14:0, C16:0, C18:1, C20:1, C22:0, C22:1, C24:1, C26:0 and C26:1 ceramide-derived species might impair PPARgamma2 transcriptional activity. These results imply that adipocytes possess the machinery needed to uptake ceramide and modify it by increasing or decreasing fatty acid chain length and unsaturation.

A relevant contribution of our study states that chronic C24:0 ceramide exposure in mice develops liver steatosis. Insulin signaling in the liver activates the lipogenic program and thus, hyperinsulinemia is the primary cause of lipid accumulation in the liver in obese individuals [65]. We have reported hyperinsulinemia states in the offspring of mothers exposed to CAF diet during fetal programming [5]. Also, hepatic steatosis can develop as a result of defective mitochondria function [66]. We identified decreased mitochondrial activity in hepatic HUH7 cells exposed to C24:0 ceramide, including defective ATP production, blunted maximal respiration, decreased fatty acid utilization, and augmented mitochondria calcium. In our study, SAT from mice treated with C24:0 ceramide and exposed to CAF diet challenge also presented decreased mitochondrial membrane potential and increased reactive oxygen species production. Also, hMSC-derived adipocytes treated with C24:0 ceramide produced C14:0, C16:0, C18:1, C20:1, C22:0, C22:1, C24:1, C26:0 and C26:1. Our data agree with previous reports confirming that C16:0 or C18:0 ceramides or ceramide synthetase 2 overexpression inhibit mitochondrial respiration in skeletal muscle [66], liver [67], brown adipose tissue [18,19] and cardiomyocytes [68]. Resembling our *in vitro* data in hepatic HUH7 cells treated with C24:0 ceramide, defective mitochondria function associates to hepatic steatosis [69] and mice exposed to high fat diet during fetal programming showed impairment of mitochondria function in liver [70], which both potentially might explain lipid accumulation in the liver of mice found in our study.

Finally, we identified that C24:0 ceramide induces ER stress in hepatic HUH7 cells evidenced by a decreased in the signal of ER-tracker and increased UPR markers, including p-eIF2, ATF6, BiP and XBP1. Excessive mitochondrial Ca + influx can be mediated by increased Ca + release from the ER during ER stress [71,72]. Ceramides activate ER stress response and disrupt mitochondria dynamics in hepatic HepG2 cells [73] and promote mitochondria fragmentation in cardiomyocytes or C2C12 cells [74,75], which correlates with *in vivo* liver steatosis following a high-fat diet challenge [17]. In fact, C16:0 ceramides activate ER stress by affecting calcium homeostasis in the ER/Golgi membrane network [76]. Given the anatomical and functional ER and mitochondria connectivity a tentative scenario might be that C24:0 ceramide promotes ER stress by a structural stiffness in the membrane of the reticle, leading to UPR activation, as was proposed [77]. ER stress is also associated with increased de novo lipogenesis trough a mechanism involving the proteolytic activation of SREBP1, which in turn increases lipogenic gene expression [78]. In line with this, our *in vitro* and *in vivo* evidence indicates that C24:0 increased SREBP1 protein abundance in hepatocytes, associated with increased lipid content.

We conclude that fetal programming by exposure to high-energy diets accumulates plasma C24:0 ceramide in the male mice offspring, which is also found highly concentrated in blood samples of obese-T2DM human subjects. C24:0 ceramide affects mitochondria and ER dynamics and function and favors ER stress-induced inflammatory and lipogenic signals. Our study highlights that C24:0 ceramide impairs adipose tissue size and promotes lipid accumulation in liver, triggering defective glucose metabolism at early stages of postnatal life.

Funding

This work was funded by the National Council of Science and Technology in Mexico (CONACYT) (Grant number: 255317 and 261420). Also, 573686 CONACYT for Roger Maldonado-Ruiz.

Data included in article/supplementary material is referenced in the article.

CRediT authorship contribution statement

Alberto Camacho-Morales: Writing – review & editing, Writing – original draft, Visualization, Validation, Supervision, Resources, Methodology, Investigation, Funding acquisition, Formal analysis, Data curation, Conceptualization. **Lilia G. Noriega:** Software, Resources, Methodology, Data curation, Conceptualization. **Adriana Sánchez-García:** Resources, Data curation. **Ivan Torre-Villalvazo:** Project administration, Methodology, Investigation, Conceptualization. **Natalia Vázquez-Manjarrez:** Resources, Investigation. **Roger Maldonado-Ruiz:** Visualization, Methodology, Investigation, Formal analysis. **Marcela Cárdenas-Tueme:** Methodology,

Investigation, Formal analysis. **Mariana Villegas-Romero:** Resources, Investigation. **Itzayana Alamilla-Martínez:** Resources, Methodology, Conceptualization. **Humberto Rodriguez-Rocha:** Validation, Methodology, Investigation. **Aracely Garcia-Garcia:** Resources, Methodology, Investigation. **Juan Carlos Corona:** Methodology, Investigation, Funding acquisition. **Armando R. Tovar:** Visualization, Validation, Investigation. **Jennifer Saville:** Methodology, Investigation, Formal analysis, Data curation. **Maria Fuller:** Resources, Methodology, Investigation. **José Gerardo Gonzalez-Gonzalez:** Supervision, Resources, Methodology, Conceptualization. **Ana María Rivas-Estilla:** Supervision, Resources, Methodology, Investigation.

Declaration of competing interest

The authors declare that they have no known competing financial interests or personal relationships that could have appeared to influence the work reported in this paper.

Acknowledgments

The authors thank M.S. Alejandra Arreola-Triana for her support on editing this manuscript. The lipidomics analysis applied in this study at the Instituto Nacional de Ciencias Médicas y nutrición Salvador Zubirán was supported by the Periodic Table of Food Initiative (PTFI) and the American Heart Association, with funding from the Rockefeller Foundation, the Foundation for Food and Agriculture Research (FFAR), and the Seerave Foundation.

Appendix A. Supplementary data

Supplementary data to this article can be found online at https://doi.org/10.1016/j.heliyon.2024.e39206.

References

[1] H. Itoh, M. Ueda, M. Suzuki, Y. Kohmura-Kobayashi, Developmental Origins of metaflammation; A bridge to the future between the DOHaD theory and evolutionary biology, Front. Endocrinol. 13 (2022), https://doi.org/10.3389/fendo.2022.839436.
[2] S. Santos, C. Monnereau, J.F. Felix, L. Duijts, R. Gaillard, V.W.V. Jaddoe, Maternal body mass index, gestational weight gain, and childhood abdominal, pericardial, and liver fat assessed by magnetic resonance imaging, Int. J. Obes. (2019), https://doi.org/10.1038/s41366-018-0186-y.
[3] R. Maldonado-Ruiz, M. Cárdenas-Tueme, L. Montalvo-Martínez, R. Vidaltamayo, L. Garza-Ocañas, D. Reséndez-Perez, A. Camacho, Priming of hypothalamic ghrelin signaling and microglia activation exacerbate feeding in rats' offspring following maternal overnutrition, Nutrients 11 (2019), https://doi.org/10.3390/nu11061241.
[4] A. Camacho-Morales, A. Caballero-Benitez, E. Vázquez-Cruz, R. Maldonado-Ruiz, M. Cárdenas-Tueme, A. Rojas-Martinez, D. Caballero-Hernández, Maternal programming by high-energy diets primes ghrelin sensitivity in the offspring of rats exposed to chronic immobilization stress, Nutr. Res. 107 (2022), https://doi.org/10.1016/j.nutres.2022.08.007.
[5] R.E. Cardenas-Perez, L. Fuentes-Mera, A.L. De La Garza, I. Torre-Villalvazo, L.A. Reyes-Castro, H. Rodriguez-Rocha, A. Garcia-Garcia, J.C. Corona-Castillo, A. R. Tovar, E. Zambrano, R. Ortiz-Lopez, J. Saville, M. Fuller, A. Camacho, Maternal overnutrition by hypercaloric diets programs hypothalamic mitochondrial fusion and metabolic dysfunction in rat male offspring, Nutr. Metab. 15 (2018), https://doi.org/10.1186/s12986-018-0279-6.
[6] G. Cruz-Carrillo, L. Montalvo-Martínez, M. Cárdenas-Tueme, S. Bernal-Vega, R. Maldonado-Ruiz, D. Reséndez-Pérez, D. Rodríguez-Ríos, G. Lund, L. Garza-Ocañas, A. Camacho-Morales, Fetal programming by methyl donors modulates central inflammation and prevents food addiction-like behavior in rats, Front. Neurosci. 14 (2020), https://doi.org/10.3389/fnins.2020.00452.
[7] A. Camacho, L. Montalvo-Martinez, R.E. Cardenas-Perez, L. Fuentes-Mera, L. Garza-Ocañas, Obesogenic diet intake during pregnancy programs aberrant synaptic plasticity and addiction-like behavior to a palatable food in offspring, Behav. Brain Res. 330 (2017), https://doi.org/10.1016/j.bbr.2017.05.014.
[8] M.C. Alexandre-Gouabau, A. David-Sochard, A.L. Royer, P. Parnet, V. Paillé, Moderate high caloric maternal diet impacts dam breast milk metabotype and offspring lipidome in a sex-specific manner, Int. J. Mol. Sci. 21 (2020), https://doi.org/10.3390/ijms21155428.
[9] L.V. Mennitti, L.M. Oyama, A.B. Santamarina, O. do Nascimento, L.P. Pisani, Influence of maternal consumption of different types of fatty acids during pregnancy and lactation on lipid and glucose metabolism of the 21-day-old male offspring in rats, Prostaglandins Leukot. Essent. Fat. Acids. 135 (2018), https://doi.org/10.1016/j.plefa.2018.07.001.
[10] C. Savva, L.A. Helguero, M. González-Granillo, T. Melo, D. Couto, B. Buyandelger, S. Gustafsson, J. Liu, M.R. Domingues, X. Li, M. Korach-André, Maternal high-fat diet programs white and brown adipose tissue lipidome and transcriptome in offspring in a sex- and tissue-dependent manner in mice, Int. J. Obes. 46 (2022), https://doi.org/10.1038/s41366-021-01060-5.
[11] J.M. Haus, S.R. Kashyap, T. Kasumov, R. Zhang, K.R. Kelly, R.A. Defronzo, J.P. Kirwan, Plasma ceramides are elevated in obese subjects with type 2 diabetes and correlate with the severity of insulin resistance, Diabetes (2009), https://doi.org/10.2337/db08-1228.
[12] C.L. Kien, J.Y. Bunn, M.E. Poynter, R. Stevens, J. Bain, O. Ikayeva, N.K. Fukagawa, C.M. Champagne, K.I. Crain, T.R. Koves, D.M. Muoio, A lipidomics analysis of the relationship between dietary fatty acid composition and insulin sensitivity in young adults, Diabetes (2013), https://doi.org/10.2337/db12-0363.
[13] L.K. Heilbronn, A.C.F. Coster, L.V. Campbell, J.R. Greenfield, K. Lange, M.J. Christopher, P.J. Meikle, D. Samocha-Bonet, The effect of short-term overfeeding on serum lipids in healthy humans, Obesity (2013), https://doi.org/10.1002/oby.20508.
[14] L. Wigger, C. Cruciani-Guglielmacci, A. Nicolas, J. Denom, N. Fernandez, F. Fumeron, P. Marques-Vidal, A. Ktorza, W. Kramer, A. Schulte, H. Le Stunff, R. Liechti, I. Xenarios, P. Vollenweider, G. Waeber, I. Uphues, R. Roussel, C. Magnan, M. Ibberson, B. Thorens, Plasma dihydroceramides are diabetes susceptibility biomarker candidates in mice and humans, Cell Rep. (2017), https://doi.org/10.1016/j.celrep.2017.02.019.
[15] S. Brachtendorf, K. El-Hindi, S. Grösch, Ceramide synthases in cancer therapy and chemoresistance, Prog. Lipid Res. 74 (2019), https://doi.org/10.1016/j.plipres.2019.04.002.
[16] S. Bernal-Vega, M. García-Juárez, A. Camacho-Morales, Contribution of ceramides metabolism in psychiatric disorders, J. Neurochem. (2023), https://doi.org/10.1111/jnc.15759.
[17] P. Hammerschmidt, D. Ostkotte, H. Nolte, M.J. Gerl, A. Jais, H.L. Brunner, H.G. Sprenger, M. Awazawa, H.T. Nicholls, S.M. Turpin-Nolan, T. Langer, M. Krüger, B. Brügger, J.C. Brüning, CerS6-Derived sphingolipids interact with mff and promote mitochondrial fragmentation in obesity, Cell (2019) 1536–1552, https://doi.org/10.1016/j.cell.2019.05.008.

[18] S.M. Turpin, H.T. Nicholls, D.M. Willmes, A. Mourier, S. Brodesser, C.M. Wunderlich, J. Mauer, E. Xu, P. Hammerschmidt, H.S. Brönneke, A. Trifunovic, G. Losasso, F.T. Wunderlich, J.W. Kornfeld, M. Blüher, M. Krönke, J.C. Brüning, Obesity-induced CerS6-dependent C16:0 ceramide production promotes weight gain and glucose intolerance, Cell Metab. 20 (2014) 678–686, https://doi.org/10.1016/j.cmet.2014.08.002.

[19] S.M. Turpin-Nolan, P. Hammerschmidt, W. Chen, A. Jais, K. Timper, M. Awazawa, S. Brodesser, J.C. Brüning, CerS1-Derived C18:0 ceramide in skeletal muscle promotes obesity-induced insulin resistance, Cell Rep. (2019), https://doi.org/10.1016/j.celrep.2018.12.031.

[20] J. Ausman, J. Abbade, L. Ermini, A. Farrell, A. Tagliaferro, M. Post, I. Caniggia, Ceramide-induced BOK promotes mitochondrial fission in preeclampsia, Cell Death Dis. 9 (2018), https://doi.org/10.1038/s41419-018-0360-0.

[21] S. Li, Y. Wu, Y. Ding, M. Yu, Z. Ai, CerS6 regulates cisplatin resistance in oral squamous cell carcinoma by altering mitochondrial fission and autophagy, J. Cell. Physiol. 233 (2018), https://doi.org/10.1002/jcp.26815.

[22] V. Parra, V. Eisner, M. Chiong, A. Criollo, F. Moraga, A. Garcia, S. Härtel, E. Jaimovich, A. Zorzano, C. Hidalgo, S. Lavandero, Changes in mitochondrial dynamics during ceramide-induced cardiomyocyte early apoptosis, Cardiovasc. Res. (2008), https://doi.org/10.1093/cvr/cvm029.

[23] A.P. Arruda, B.M. Pers, G. Parlakgül, E. Güney, K. Inouye, G.S. Hotamisligil, Chronic enrichment of hepatic endoplasmic reticulum-mitochondria contact leads to mitochondrial dysfunction in obesity, Nat. Med. (2014), https://doi.org/10.1038/nm.3735.

[24] B. Díaz, L. Fuentes-Mera, A. Tovar, T. Montiel, L. Massieu, H.G. Martínez-Rodríguez, A. Camacho, Saturated lipids decrease mitofusin 2 leading to endoplasmic reticulum stress activation and insulin resistance in hypothalamic cells, Brain Res. 1627 (2015), https://doi.org/10.1016/j.brainres.2015.09.014.

[25] M. Schneeberger, M.O. Dietrich, D. Sebastián, M. Imbernón, C. Castaño, A. Garcia, Y. Esteban, A. Gonzalez-Franquesa, I.C. Rodríguez, A. Bortolozzi, P.M. Garcia-Roves, R. Gomis, R. Nogueiras, T.L. Horvath, A. Zorzano, M. Claret, Mitofusin 2 in POMC neurons connects ER stress with leptin resistance and energy imbalance, Cell (2013), https://doi.org/10.1016/j.cell.2013.09.003.

[26] J.L. Saben, A.L. Boudoures, Z. Asghar, A. Thompson, A. Drury, W. Zhang, M. Chi, A. Cusumano, S. Scheaffer, K.H. Moley, Maternal metabolic syndrome programs mitochondrial dysfunction via germline changes across three generations, Cell Rep. (2016), https://doi.org/10.1016/j.celrep.2016.05.065.

[27] C.A. Pileggi, C.P. Hedges, S.A. Segovia, J.F. Markworth, B.R. Durainayagam, C. Gray, X.D. Zhang, M.P.G. Barnett, M.H. Vickers, A.J.R. Hickey, C.M. Reynolds, D. Cameron-Smith, Maternal high fat diet alters skeletal muscle mitochondrial catalytic activity in adult male rat offspring, Front. Physiol. (2016), https://doi.org/10.3389/fphys.2016.00546.

[28] B. Chaurasia, S.A. Summers, Ceramides in metabolism: key lipotoxic players, Annu. Rev. Physiol. 83 (2021), https://doi.org/10.1146/annurev-physiol-031620-093815.

[29] S. Carobbio, V. Pellegrinelli, A. Vidal-Puig, Adipose tissue function and expandability as determinants of lipotoxicity and the metabolic syndrome, in: Adv. Exp. Med. Biol. (2017), https://doi.org/10.1007/978-3-319-48382-5_7.

[30] B. Gustafson, U. Smith, Regulation of white adipogenesis and its relation to ectopic fat accumulation and cardiovascular risk, Atherosclerosis 241 (2015) 27–35, https://doi.org/10.1016/j.atherosclerosis.2015.04.812.

[31] D.J. Powell, S. Turban, A. Gray, E. Hajduch, H.S. Hundal, Intracellular ceramide synthesis and protein kinase Cζ activation play an essential role in palmitate-induced insulin resistance in rat L6 skeletal muscle cells, Biochem. J. 382 (2004), https://doi.org/10.1042/BJ20040139.

[32] M.J. Watt, A. Hevener, G.I. Lancaster, M.A. Febbraio, Ciliary neurotrophic factor prevents acute lipid-induced insulin resistance by attenuating ceramide accumulation and phosphorylation of c-Jun N-terminal kinase in peripheral tissues, Endocrinology 147 (2006), https://doi.org/10.1210/en.2005-1074.

[33] A.L. de la Garza, M.A. Garza-Cuellar, I.A. Silva-Hernandez, R.E. Cardenas-Perez, L.A. Reyes-Castro, E. Zambrano, B. Gonzalez-Hernandez, L. Garza-Ocañas, L. Fuentes-Mera, A. Camacho, Maternal flavonoids intake reverts depression-like behaviour in rat female offspring, Nutrients 11 (2019), https://doi.org/10.3390/nu11030572.

[34] G. Cruz-Carrillo, L.A. Trujillo-Villarreal, D. Ángeles-Valdez, L. Concha, E.A. Garza-Villarreal, A. Camacho-Morales, Prenatal cafeteria diet primes anxiety-like behavior associated to defects in volume and diffusion in the fimbria-fornix of mice offspring, Neuroscience 511 (2023), https://doi.org/10.1016/j.neuroscience.2022.12.021.

[35] L. Montalvo-Martínez, G. Cruz-Carrillo, R. Maldonado-Ruiz, M. Cárdenas-Tueme, S. Bernal-Vega, L. Garza-Ocañas, R. Ortiz-López, D. Reséndez-Pérez, A. Camacho-Morales, Maternal high-dense diet programs interferon type I signaling and microglia complexity in the nucleus accumbens shell of rats showing food addiction-like behavior, Neuroreport 33 (2022), https://doi.org/10.1097/WNR.0000000000001784.

[36] L. Montalvo-Martínez, G. Cruz-Carrillo, R. Maldonado-Ruiz, L.A. Trujillo-Villarreal, M. Cardenas-Tueme, R. Viveros-Contreras, R. Ortiz-López, A. Camacho-Morales, Transgenerational susceptibility to food addiction-like behavior in rats associates to a decrease of the anti-inflammatory IL-10 in plasma, Neurochem. Res. 47 (2022), https://doi.org/10.1007/s11064-022-03660-7.

[37] R. Maldonado-Ruiz, L.A. Trujillo-Villarreal, L. Montalvo-Martínez, O.F. Mercado-Gómez, V. Arriaga-Ávila, L. Garza-Ocañas, R. Ortiz-López, E.A. Garza-Villarreal, R. Guevara-Guzmán, A. Camacho-Morales, MCP-1 signaling disrupts social behavior by modulating brain volumetric changes and microglia morphology, Mol. Neurobiol. 59 (2022), https://doi.org/10.1007/s12035-021-02649-7.

[38] C. Giles, R. Takechi, N.A. Mellett, P.J. Meikle, S. Dhaliwal, J.C. Mamo, Differential regulation of sphingolipid metabolism in plasma, hippocampus, and cerebral cortex of mice administered sphingolipid modulating agents, J. Neurochem. 141 (2017), https://doi.org/10.1111/jnc.13964.

[39] M. Fuller, J. Szer, S. Stark, J.M. Fletcher, Rapid, single-phase extraction of glucosylsphingosine from plasma: a universal screening and monitoring tool, Clin. Chim. Acta (2015), https://doi.org/10.1016/j.cca.2015.07.026.

[40] J.T. Saville, H.N. Thai, R.J. Lehmann, A.L.K. Derrick-Roberts, M. Fuller, Subregional brain distribution of simple and complex glycosphingolipids in the mucopolysaccharidosis type I (Hurler syndrome) mouse: impact of diet, J. Neurochem. (2017), https://doi.org/10.1111/jnc.13976.

[41] A. Camacho, J.C. Segoviano-Ramírez, A. Sánchez-Garcia, J. De Jesus Herrera-De La Rosa, J. García-Juarez, C.A. Hernandez-Puente, G. Calvo-Anguiano, S. R. Maltos-Uro, A. Olguin, G. Gojon-Romanillos, G. Gojon-Zorrilla, R. Ortiz-Lopez, Tyrphostin AG17 inhibits adipocyte differentiation in vivo and in vitro, Lipids Health Dis. (2018), https://doi.org/10.1186/s12944-018-0784-7.

[42] C.E. Hagberg, Q. Li, M. Kutschke, D. Bhowmick, E. Kiss, I.G. Shabalina, M.J. Harms, O. Shilkova, V. Kozina, J. Nedergaard, J. Boucher, A. Thorell, K.L. Spalding, Flow cytometry of mouse and human adipocytes for the analysis of browning and cellular heterogeneity, Cell Rep. 24 (2018), https://doi.org/10.1016/j.celrep.2018.08.006.

[43] E.G. Bligh, W.J. Dyer, A rapid method of total lipid extraction and purification, Can. J. Biochem. Physiol. 37 (1959), https://doi.org/10.1139/o59-099.

[44] B. Su, L.F. Bettcher, W.Y. Hsieh, D. Hornburg, M.J. Pearson, N. Blomberg, M. Giera, M.P. Snyder, D. Raftery, S.J. Bensinger, K.J. Williams, A DMS Shotgun lipidomics workflow application to facilitate high-throughput, comprehensive lipidomics, J. Am. Soc. Mass Spectrom. 32 (2021), https://doi.org/10.1021/jasms.1c00203.

[45] S. Shin, J. Kim, J.Y. Lee, J. Kim, C.M. Oh, Mitochondrial quality control: its role in metabolic dysfunction-associated steatotic liver disease (MASLD), J. Obes. Metab. Syndr. 32 (2023), https://doi.org/10.7570/jomes23054.

[46] Q. Chen, A. Kovilakath, J. Allegood, J. Thompson, Y. Hu, L.A. Cowart, E.J. Lesnefsky, Endoplasmic reticulum stress and mitochondrial dysfunction during aging: role of sphingolipids, Biochim. Biophys. Acta - Mol. Cell Biol. Lipids. 1868 (2023), https://doi.org/10.1016/j.bbalip.2023.159366.

[47] J. Ren, Y. Bi, J.R. Sowers, C. Hetz, Y. Zhang, Endoplasmic reticulum stress and unfolded protein response in cardiovascular diseases, Nat. Rev. Cardiol. 18 (2021), https://doi.org/10.1038/s41569-021-00511-w.

[48] P. Wiesner, K. Leidl, A. Boettcher, G. Schmitz, G. Liebisch, Lipid profiling of FPLC-separated lipoprotein fractions by electrospray ionization tandem mass spectrometry, J. Lipid Res. (2009), https://doi.org/10.1194/jlr.d800028-jlr200.

[49] K.H. Pietiläinen, M. Sysi-Aho, A. Rissanen, T. Seppänen-Laakso, H. Yki-Järvinen, J. Kaprio, M. Orešič, Acquired obesity is associated with changes in the serum lipidomic profile independent of genetic effects - a monozygotic twin study, PLoS One (2007), https://doi.org/10.1371/journal.pone.0000218.

[50] A. Ribel-Madsen, R. Ribel-Madsen, K.F. Nielsen, S. Brix, A.A. Vaag, C. Brøns, Plasma ceramide levels are altered in low and normal birth weight men in response to short-term high-fat overfeeding, Sci. Rep. 8 (2018) 1–11, https://doi.org/10.1038/s41598-018-21419-5.

[51] H. Jiang, F.F. Hsu, M.S. Farmer, L.R. Peterson, J.E. Schaffer, D.S. Ory, X. Jiang, Development and validation of LC-MS/MS method for determination of very long acyl chain (C22:0 and C24:0) ceramides in human plasma, Anal. Bioanal. Chem. (2013), https://doi.org/10.1007/s00216-013-7166-9.

[52] T. Kasumov, T.P.J. Solomon, C. Hwang, H. Huang, J.M. Haus, R. Zhang, J.P. Kirwan, Improved insulin sensitivity after exercise training is linked to reduced plasma C14:0 ceramide in obesity and type 2 diabetes, Obesity (2015), https://doi.org/10.1002/oby.21117.
[53] B.C. Bergman, J.T. Brozinick, A. Strauss, S. Bacon, A. Kerege, H.H. Bui, P. Sanders, P. Siddall, M.S. Kuo, L. Perreault, Serum sphingolipids: relationships to insulin sensitivity and changes with exercise in humans, Am. J. Physiol. Endocrinol. Metab. (2015), https://doi.org/10.1152/ajpendo.00134.2015.
[54] J.N. Jones Buie, S.M. Hammad, P.J. Nietert, G. Magwood, R.J. Adams, L. Bonilha, C. Sims-Robinson, Differences in plasma levels of long chain and very long chain ceramides between African Americans and whites: an observational study, PLoS One (2019), https://doi.org/10.1371/journal.pone.0216213.
[55] M. Mamtani, P.J. Meikle, H. Kulkarni, J.M. Weir, C.K. Barlow, J.B. Jowett, C. Bellis, T.D. Dyer, L. Almasy, M.C. Mahaney, R. Duggirala, A.G. Comuzzie, J. Blangero, J.E. Curran, Plasma dihydroceramide species associate with waist circumference in Mexican American families, Obesity (2014), https://doi.org/10.1002/oby.20598.
[56] C.A. Pomar, R. Van Nes, J. Sánchez, C. Picó, J. Keijer, A. Palou, Maternal consumption of a cafeteria diet during lactation in rats leads the offspring to a thin-outside-fat-inside phenotype, Int. J. Obes. (2017), https://doi.org/10.1038/ijo.2017.42.
[57] A.C. Reichelt, M.J. Morris, R.F. Westbrook, Cafeteria diet impairs expression of sensory-specific satiety and stimulus-outcome learning, Front. Psychol. (2014), https://doi.org/10.3389/fpsyg.2014.00852.
[58] T. Litzenburger, E.K. Huber, K. Dinger, R. Wilke, C. Vohlen, J. Selle, M. Kadah, T. Persigehl, C. Heneweer, J. Dotsch, M.A.A. Alcazar, Maternal high-fat diet induces long-term obesity with sex-dependent metabolic programming of adipocyte differentiation, hypertrophy and dysfunction in the offspring, Clin. Sci. 134 (2020), https://doi.org/10.1042/CS20191229.
[59] N. Turner, G.M. Kowalski, S.J. Leslie, S. Risis, C. Yang, R.S. Lee-Young, J.R. Babb, P.J. Meikle, G.I. Lancaster, D.C. Henstridge, P.J. White, E.W. Kraegen, A. Marette, G.J. Cooney, M.A. Febbraio, C.R. Bruce, Distinct patterns of tissue-specific lipid accumulation during the induction of insulin resistance in mice by high-fat feeding, Diabetologia 56 (2013), https://doi.org/10.1007/s00125-013-2913-1.
[60] D. Gosejacob, P.S. Jäger, K. Vom Dorp, M. Frejno, A.C. Carstensen, M. Köhnke, J. Degen, P. Dörmann, M. Hoch, Ceramide synthase 5 is essential to maintain C16:0-Ceramide pools and contributes to the development of diet-induced obesity, J. Biol. Chem. (2016), https://doi.org/10.1074/jbc.M115.691212.
[61] J.Y. Xia, W.L. Holland, C.M. Kusminski, K. Sun, A.X. Sharma, M.J. Pearson, A.J. Sifuentes, J.G. McDonald, R. Gordillo, P.E. Scherer, Targeted induction of ceramide degradation leads to improved systemic metabolism and reduced hepatic steatosis, Cell Metab. 22 (2015), https://doi.org/10.1016/j.cmet.2015.06.007.
[62] P. Hammerschmidt, J.C. Brüning, Contribution of specific ceramides to obesity-associated metabolic diseases, Cell. Mol. Life Sci. 79 (2022), https://doi.org/10.1007/s00018-022-04401-3.
[63] A. Pirraco, J. Relat, I. Cuadrado, V. Pellegrinelli, Increased dihydroceramide/ceramide ratio mediated by defective expression of degs1 impairs adipocyte differentiation and function. Nuria Adipose Tissue Dysfunction Is an Important Determinant of Obesity-Associated Lipid Induced Metabolic Complications, 2014, pp. 1–42.
[64] F. Xu, C.C. Yang, C. Gomillion, K.J.L. Burg, Effect of ceramide on mesenchymal stem cell differentiation toward adipocytes, Appl. Biochem. Biotechnol. (2010), https://doi.org/10.1007/s12010-008-8505-8.
[65] G.I. Smith, M. Shankaran, M. Yoshino, G.G. Schweitzer, M. Chondronikola, J.W. Beals, A.L. Okunade, B.W. Patterson, E. Nyangau, T. Field, C.B. Sirlin, S. Talukdar, M.K. Hellerstein, S. Klein, Insulin resistance drives hepatic de novo lipogenesis in nonalcoholic fatty liver disease, J. Clin. Invest. 130 (2020), https://doi.org/10.1172/JCI134165.
[66] L. Perreault, S.A. Newsom, A. Strauss, A. Kerege, D.E. Kahn, K.A. Harrison, J.K. Snell-Bergeon, T. Nemkov, A. D'Alessandro, M.R. Jackman, P.S. MacLean, B. C. Bergman, Intracellular localization of diacylglycerols and sphingolipids influences insulin sensitivity and mitochondrial function in human skeletal muscle, JCI Insight (2018), https://doi.org/10.1172/jci.insight.96805.
[67] B. Chaurasia, T.S. Tippetts, R.M. Monibas, J. Liu, Y. Li, L. Wang, J.L. Wilkerson, C. Rufus Sweeney, R.F. Pereira, D.H. Sumida, J. Alan Maschek, J.E. Cox, V. Kaddai, G.I. Lancaster, M.M. Siddique, A. Poss, M. Pearson, S. Satapati, H. Zhou, D.G. McLaren, S.F. Previs, Y. Chen, Y. Qian, A. Petrov, M. Wu, X. Shen, J. Yao, C.N. Nunes, A.D. Howard, L. Wang, M.D. Erion, J. Rutter, W.L. Holland, D.E. Kelley, S.A. Summers, Targeting a ceramide double bond improves insulin resistance and hepatic steatosis, Science (2019) 365, https://doi.org/10.1126/science.aav3722.
[68] B.A. Law, X. Liao, K.S. Moore, A. Southard, P. Roddy, R. Ji, Z. Szulc, A. Bielawska, P.C. Schulze, L.A. Cowart, Lipotoxic very-long-chain ceramides cause mitochondrial dysfunction, oxidative stress, and cell death in cardiomyocytes, FASEB J. (2018), https://doi.org/10.1096/fj.201700300R.
[69] K.G. Eriksen, E.J. Radford, M.J. Silver, A.J.C. Fulford, R. Wegmüller, A.M. Prentice, Influence of intergenerational in utero parental energy and nutrient restriction on offspring growth in rural Gambia, FASEB J. (2017), https://doi.org/10.1096/fj.201700017R.
[70] P.C. De Velasco, G. Chicaybam, D.M. Ramos-Filho, R.M.A.R. Dos Santos, C. Mairink, F.L.C. Sardinha, T. El-Bacha, A. Galina, M.D.G. Tavares-Do-Carmo, Maternal intake of trans-unsaturated or interesterified fatty acids during pregnancy and lactation modifies mitochondrial bioenergetics in the liver of adult offspring in mice, Br. J. Nutr. 118 (2017), https://doi.org/10.1017/S0007114517001817.
[71] G. Csordás, D. Weaver, G. Hajnóczky, Endoplasmic reticulum–mitochondrial contactology: structure and signaling functions, Trends Cell Biol. 28 (2018), https://doi.org/10.1016/j.tcb.2018.02.009.
[72] A. Deniaud, O. Sharaf El Dein, E. Maillier, D. Poncet, G. Kroemer, C. Lemaire, C. Brenner, Endoplasmic reticulum stress induces calcium-dependent permeability transition, mitochondrial outer membrane permeabilization and apoptosis, Oncogene 27 (2008), https://doi.org/10.1038/sj.onc.1210638.
[73] H.J. Maeng, J.H. Song, G.T. Kim, Y.J. Song, K. Lee, J.Y. Kim, T.S. Park, Celecoxib-mediated activation of endoplasmic reticulum stress induces de novo ceramide biosynthesis and apoptosis in hepatoma HepG2 cells, BMB Rep (2017), https://doi.org/10.5483/BMBRep.2017.50.3.197.
[74] M.E. Smith, T.S. Tippetts, E.S. Brassfield, B.J. Tucker, A. Ockey, A.C. Swensen, T.S. Anthonymuthu, T.D. Washburn, D.A. Kane, J.T. Prince, B.T. Bikman, Mitochondrial fission mediates ceramide-induced metabolic disruption in skeletal muscle, Biochem. J. (2013), https://doi.org/10.1042/bj20130807.
[75] S. Dadsena, S. Bockelmann, J.G.M. Mina, D.G. Hassan, S. Korneev, G. Razzera, H. Jahn, P. Niekamp, D. Müller, M. Schneider, F.G. Tafesse, S.J. Marrink, M. N. Melo, J.C.M. Holthuis, Ceramides bind VDAC2 to trigger mitochondrial apoptosis, Nat. Commun. (2019), https://doi.org/10.1038/s41467-019-09654-4.
[76] C.E. Senkal, S. Ponnusamy, Y. Manevich, M. Meyers-Needham, S.A. Saddoughi, A. Mukhopadyay, P. Dent, J. Bielawski, B. Ogretmen, Alteration of ceramide synthase 6/C 16-ceramide induces activating transcription factor 6-mediated Endoplasmic Reticulum (ER) stress and apoptosis via perturbation of cellular Ca 2 + and ER/golgi membrane network, J. Biol. Chem. (2011), https://doi.org/10.1074/jbc.M111.287383.
[77] C.T. Hsieh, J.H. Chuang, W.C. Yang, Y. Yin, Y. Lin, Ceramide inhibits insulin-stimulated Akt phosphorylation through activation of Rheb/mTORC1/S6K signaling in skeletal muscle, Cell. Signal. (2014), https://doi.org/10.1016/j.cellsig.2014.03.004.
[78] D.L. Fang, Y. Wan, W. Shen, J. Cao, Z.X. Sun, H.H. Yu, Q. Zhang, W.H. Cheng, J. Chen, B. Ning, Endoplasmic reticulum stress leads to lipid accumulation through upregulation of SREBP-1c in normal hepatic and hepatoma cells, Mol. Cell. Biochem. 381 (2013), https://doi.org/10.1007/s11010-013-1694-7.